

หมึกนำไฟฟ้าจากอนุภาคเงินระดับนาโนเมตรที่สามารถชินเทอร์ได้ที่อุณหภูมิห้อง



นายชุตินันท์ เลิศวชิรไพบุลย์

ศูนย์วิจัยทรัพยากร

วิทยานพนธ์นี้เป็นส่วนหนึ่งของการศึกษาตามหลักสูตรปริญญาวิทยาศาสตรมหาบัณฑิต

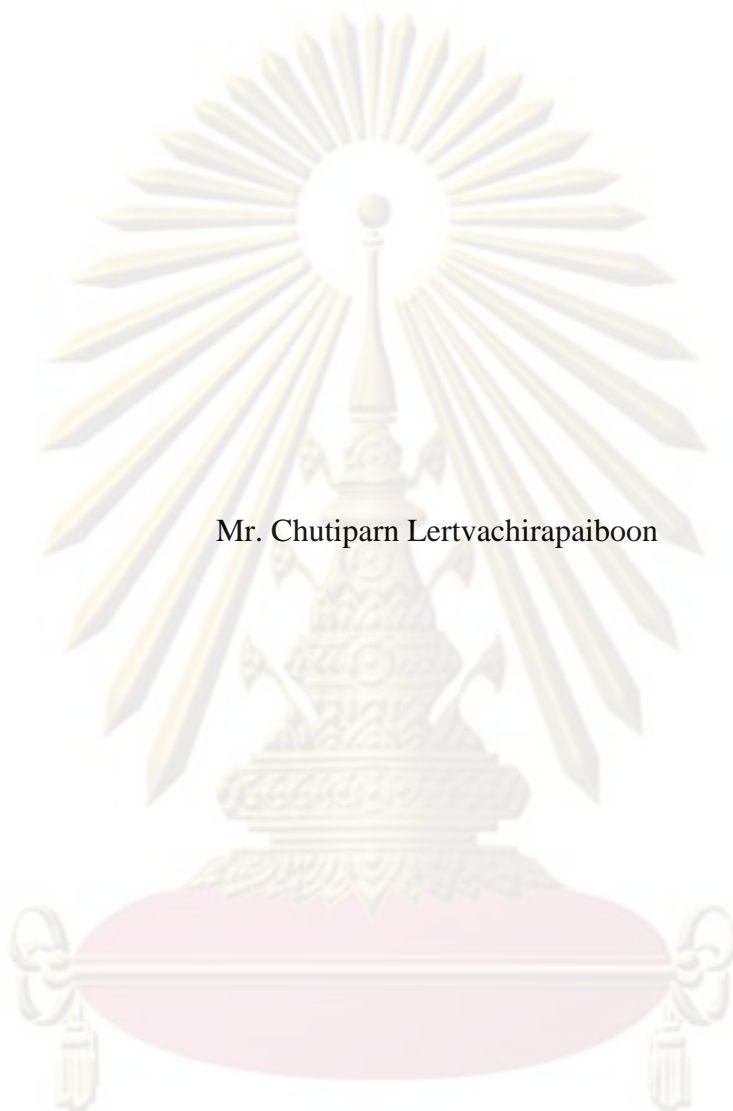
สาขาวิชาเคมี ภาควิชาเคมี

คณะวิทยาศาสตร์ จุฬาลงกรณ์มหาวิทยาลัย

ปีการศึกษา 2552

ลิขสิทธิ์ของจุฬาลงกรณ์มหาวิทยาลัย

ROOM-TEMPERATURE-SINTERED CONDUCTIVE INK MADE OF
SILVER NANOPARTICLES



Mr. Chutiparn Lertvachirapaiboon

A Thesis Submitted in Partial Fulfillment of the Requirements
for the Degree of Master of Science Program in Chemistry

Department of Chemistry

Faculty of Science


Chulalongkorn University

Academic Year 2009

Copyright of Chulalongkorn University


Thesis Title ROOM-TEMPERATURE-SINTERED CONDUCTIVE INK MADE
OF SILVER NANOPARTICLES
By Mr.Chutiparn Lertvachirapaiboon
Field of Study Chemistry
Thesis Advisor Associate Professor Sanong Ekgasit, Ph.D.
Thesis Co-advisor Associate Professor Chuchaat Thammacharoen

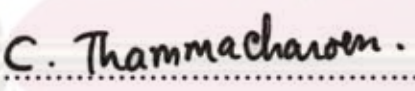
Accepted by the Faculty of Science, Chulalongkorn University in Partial
Fulfillment of the Requirements for Master's degree

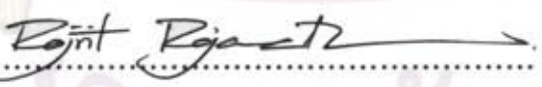

..... Dean of the Faculty of Science
(Professor Supot Hammongbua, Ph.D.)

THESIS COMMITTEE


..... Chairman
(Associate Professor Sirirat Kokpol, Ph.D.)


..... Thesis Advisor
(Associate Professor Sanong Ekgasit, Ph.D.)


..... Thesis Co-Advisor
(Associate Professor Chuchaat Thammacharoen)


..... Examiner
(Rojrit Rojanathanes, Ph.D.)


..... External Examiner
(Assistant Professor Toemsak Srihirin, Ph.D.)

ศูนย์วิจัยทรัพยากร
จุฬาลงกรณ์มหาวิทยาลัย

ชุตินันท์ เดิศวธิ์ ไพบูลย์ : หมึกนำไฟฟ้าจากอนุภาคเงินระดับนาโนเมตรที่สามารถซินเทอร์ไว้ได้ที่อุณหภูมิห้อง (ROOM-TEMPERATURE-SINTERED CONDUCTIVE INK MADE OF SILVER NANOPARTICLES) อ.ที่ปรึกษาวิทยานิพนธ์หลัก: รศ. ดร.สนอง เอกสิทธิ์, อ.ที่ปรึกษาวิทยานิพนธ์ร่วม: รศ.ชูชาติ ธรรมเจริญ, 55 หน้า.

หมึกนำไฟฟ้าจากอนุภาคเงินระดับนาโนเมตรพัฒนาขึ้นเพื่อใช้กับการพิมพ์ในรูปแบบต่าง ๆ เช่น การพิมพ์แบบประทับ การพิมพ์แบบสกรีน การพิมพ์แบบครอปออนดีมานด์ (drop-on-demand) และ การใช้เป็นหมึกของปากกานำไฟฟ้า หมึกนำไฟฟ้าจากอนุภาคเงินระดับนาโนเมตรสามารถสังเคราะห์ได้จากเกลือซิลเวอร์ไนเตรดทำปฏิกิริยากับโซเดียมบอโรไฮไดรด์ อนุภาคเงินที่สังเคราะห์ได้เป็นคอลลอยด์ของอนุภาคเงินความเข้มข้นสูง และมีเสถียรภาพ เมื่อความเข้มข้นของหมึกนำไฟฟ้าถูกเจือจางเป็น 1 ส่วนในล้านส่วนเพื่อศึกษาขนาดของอนุภาค จากกล้องจุลทรรศน์แบบใช้แรงอะตอม (atomic force microscope) พบว่าอนุภาคเงินที่สังเคราะห์ได้มีขนาด 5-30 นาโนเมตร แต่เมื่อหมึกนำไฟฟ้าความเข้มข้นสูง (100,000 ส่วนในล้านส่วน) แห้งบนวัสดุรองรับแล้วขนาดของอนุภาคเงินโดยเฉลี่ยคือ 100 นาโนเมตร อนุภาคเงินในหมึกนำไฟฟ้าหลังจากแห้งบนวัสดุรองรับแล้วสามารถซินเทอร์จากอนุภาคเงินขนาดเล็กเป็นอนุภาคเงินที่มีขนาดใหญ่มากขึ้น ได้ที่อุณหภูมิห้อง หลังจากหมึกนำไฟฟ้าแห้งบนวัสดุรองรับแล้วจะสามารถแสดงสมบัติการนำไฟฟ้าได้ทันที ปฏิกิริยาการซินเทอร์ยังช่วยให้หมึกนำไฟฟ้าสามารถแสดงสมบัติการนำไฟฟ้าที่ดีขึ้น หมึกนำไฟฟ้าจากอนุภาคเงินระดับนาโนเมตรที่สามารถซินเทอร์ไว้ได้ที่อุณหภูมิห้องสามารถใช้ได้กับวัสดุรองรับที่สลายตัวได้ง่ายเมื่อได้รับความร้อน เช่น พลาสติกพอลิเมอร์ และ กระดาษ พิล์มของอนุภาคเงินหลังจากแห้งบนวัสดุรองรับสามารถปรับปรุงให้นำไฟฟ้าได้ดีขึ้น โดยการให้ความร้อน หรือ การขจัด

ศูนย์วิทยทรัพยากร

จุฬาลงกรณ์มหาวิทยาลัย

ภาควิชา.....เคมี.....ลายมือชื่อนิติศ.....ชุตินันท์ ไพบูลย์

สาขาวิชา.....เคมี.....ลายมือชื่ออาจารย์ที่ปรึกษาวิทยานิพนธ์หลัก.....อ.สนอง

ปีการศึกษา.....2552.....ลายมือชื่ออาจารย์ที่ปรึกษาวิทยานิพนธ์ร่วม.....อ.ชูชาติ

5072261723 : MAJOR CHEMISTRY

KEYWORDS : SILVER NANOPARTICLES / CONDUCTIVE INK / SINTERING

CHUTIPARN LERTVACHIRAPAIBOON : ROOM-TEMPERATURE-SINTERED CONDUCTIVE INK MADE OF SILVER NANOPARTICLES.
 THESIS ADVISOR: ASSOC. PROF. SANONG EKGASIT, PH.D., THESIS CO-ADVISOR: ASSOC. PROF. CHUCHAAT THAMMACHAROEN, 55 pp.

Conductive ink made of silver nanoparticles was developed for stamp printing, screen printing, drop-on-demand printing, and conductive line via a conductive pen. The conductive silver ink was synthesized by chemical reduction of silver salt solution with sodium borohydride. The obtained colloid of silver nanoparticles were highly concentrated and highly stabilized. When concentration of conductive silver ink was dilute to 1 ppm, the topographic image from atomic force microscope (AFM) showed silver particles size in the range of 5-30 nm. However, after a high concentration conductive ink (100,000 ppm) was deposited and dried on substrate under the ambient condition, the average size of silver particles 100 nm. Silver nanoparticles could sinter to be the larger particles at room temperature. After conductive silver ink was deposited and dried on substrate, the high silver load and sintering phenomenon enable electrical conductivity. The silver ink could be applied on thermal-sensitive substrate such as thin polymer film and paper without deforming or destroying the substrate. The conductivity of silver film could be improved by thermal treatment or by mechanical rubbing.

Department of study..... Chemistry..... Student's signature..... *ชุตินันท์ เจริญทรัพย์*
 Field of study..... Chemistry..... Advisor's signature..... *ดร. ชวน*
 Academic year..... 2009..... Co-Advisor's signature..... *อ. ชวน*

ACKNOWLEDGEMENTS

I would like to express my sincere gratitude to my thesis advisor, Associate Professor Dr. Sanong Ekgasit and my thesis co-advisor Associate Professor Chuchaat Thammacharoen for wholeheartedly provide the useful guidance, understanding, training and teaching the theoretical background and technical skills during my research.

I would like to thank Associate Professor Dr. Sirirat Kokpol, Dr. Rojrit Rojanathanes, and Assistant Professor Dr. Toemsak Srihirin for usefully substantial suggestions as the thesis committee.

Warmest thanks to my friends, my colleagues and organization: Sensor Research Unit, Department of Chemistry, Faculty of Science, Chulalongkorn University, and all good friends for the suggestions and spiritual supports through out this research.

Partial financial support from National Research Council of Thailand (NRCT), Center of Innovative Nanotechnology (CIN), Center for Petroleum, Petrochemicals, and Advanced Materials, and CHEMICAL INNOVATION CO., LTD.

Whatever shortcomings in the thesis remain, they are the sole responsibility of the author.

Above all, I am profoundly grateful to my parents and endearing family for all their loves, understanding, support, and encouragement during the whole period of my study.

CONTENTS

	Page
ABSTRACT IN THAI.....	iv
ABSTRACT IN ENGLISH.....	v
ACKNOWLEDGEMENTS.....	vi
CONTENTS.....	vii
LIST OF FIGURES.....	x
LIST OF TABLES.....	xiii
LIST OF ABBREVIATIONS.....	xiv
LIST OF SYMBOLS.....	xv
CHAPTER I INTRODUCTION.....	1
1.1 Conductive ink made of silver nanoparticles.....	1
1.2 The objectives.....	2
1.3 Scopes of research.....	2
CHAPTER II THEORETICAL BACKGROUND.....	3
2.1 Silver nanoparticles.....	3
2.2 Size effect in nanochemistry.....	4
2.2.1 Physical property.....	4
2.2.2 Optical property.....	4
2.2.3 Thermal property: melting point.....	5
2.3 Sintering phenomenon.....	8
2.3.1 Surface area change mechanism.....	10
2.3.2 Rearrangement mechanism.....	11
2.3.3 Effect of sintering on resistivity.....	13

2.4 Synthesis of silver nanoparticles.....	15
2.4.1 Chemical reductions.....	15
2.4.2 Photochemical and radiation-chemical reduction.....	17
2.4.1 Physical method.....	18
2.4.1 Stabilizer.....	20
2.5 Silver nanoparticles as conductive ink.....	21
2.6 Characterization techniques.....	22
2.6.1 Atomic force microscopy.....	22
2.6.2 Transmission electron spectroscopy.....	24
2.6.3 Four-point probe measurement.....	25
2.6.4 Attenuated Total Reflection Fourier Transform Infrared (ATR FT-IR) spectroscopy.....	26
2.6.5 UV-Visible spectroscopy.....	26
 CHAPTER III EXPERIMENT.....	 27
3.1 Chemicals and materials.....	27
3.2 Silver nanoparticles synthesis method for conductive ink.....	27
3.3 The effect of stabilizer concentration on the size of silver nanoparticles.....	29
3.4 Sintering phenomenon of conductive ink made of silver nanoparticles.....	29
3.5 Characterization conductive silver ink.....	30
3.5.1 Atomic force microscopy.....	30
3.5.2 Transmission electron spectroscopy.....	30
3.5.3 Four-point probe measurement.....	31
3.5.4 Attenuated Total Reflection Fourier Transform Infrared (ATR FT-IR) spectroscopy.....	31
3.5.5 UV-Visible spectroscopy.....	31

CHAPTER IV RESULTS AND DISCUSSION.....	32
4.1 Silver nanoparticles synthesis method as conductive ink.....	32
4.2 The effect of stabilizer concentration on the size of silver nanoparticles.....	37
4.3 Sintering phenomenon of conductive ink made of silver nanoparticles.....	42
CHAPTER V CONCLUSION.....	47
REFERENCES.....	48
CURRICULUM VITAE.....	52



ศูนย์วิทยทรัพยากร
จุฬาลงกรณ์มหาวิทยาลัย

LIST OF FIGURES

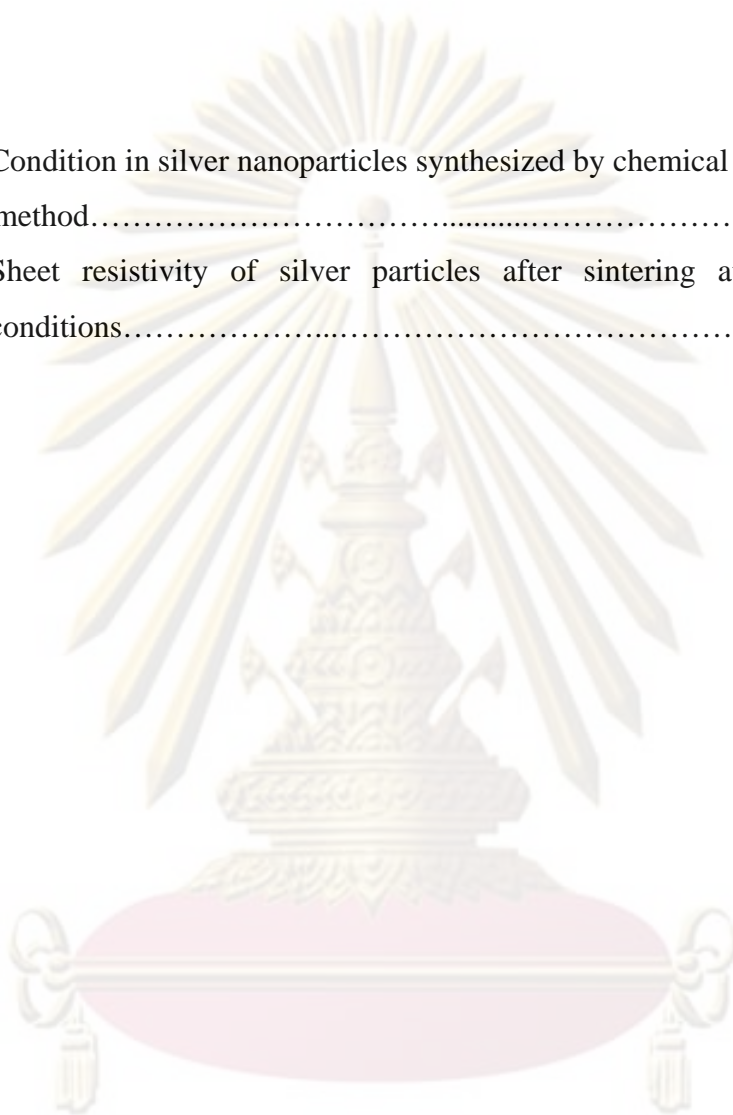
Figure	Page
2.1 Dependence of gold melting point on the particles size.....	8
2.2 Schematic diagram of sintering mechanism of particles: (A) surface area change mechanism and (B) rearrangement mechanism.....	9
2.3 Schematic diagram of sintering process between two particles.....	9
2.4 Schematic diagram of diffusion step between two particles, step 1 and 2 are lattice and surface diffusion mechanisms, respectively. These two steps do not produce any shrinkage. Step 3 and 4 are densification, center of particles approach to one another. These two steps are through-lattice diffusion and grain boundary diffusion.....	13
2.5 Resistivity as a function of linear shrinkage at 150 °C predicted by the shrinkage model versus experiment data.....	15
2.6 Schematic diagram for the preparation of silver nanoparticles by inert gas condensation (IGC) method. The pure inert gas (He or Ar) flows into the chamber and the source metal is vaporized into the flowing inert gas. As a result, nanoparticles are formed on suitable medium such as metal filter.....	18
2.7 Schematic diagram for experimental set-up for colloid preparation by laser ablation in solution. Metal nanoparticles can be produced by irradiating metal sheet with intense laser in liquid solution with the present of stabilizer. Interaction between laser and metal sheet resulted in ablation. The particles size can be controlled by changing the laser intensity and wavelength.....	19
2.8 Schematic diagram for experimental setup of spray pyrolysis. The metal salt solution is atomized into droplets and sent through a hot reactor. Then, the metal salts decompose to form the particles.....	19

Figure	Page
2.9 Schematic diagrams of (A) electrostatic stabilization and (B) steric hindrance.....	20
2.10 Schematic diagram of force curve on an ideal non-deformable material. The deflection of the cantilever is a function of the vertical of the sample during an approach-retract cycle.....	22
2.11 Schematic diagram of the atomic force microscope.....	23
2.12 Schematic diagram of transmission electron microscope (TEM).....	25
3.1 Apparatus for synthesis of conductive silver ink.....	28
3.2 Seiko SPA-400 atomic force microscope.....	30
3.3 Ocean Optics Portable UV-Visible spectrometer.....	31
4.1 UV-Visible spectrum of supernatant at (A) $R = 0.7$, (B) $R = 0.9$, and (C) $R = 1.0$. The (---) represent supernatant before adding NaBH_4 and (—) represent supernatant after adding NaBH_4	33
4.2 FT-IR spectrum of (A) supernatant, (B) washing solution and (C) conductive silver ink.	34
4.3 TEM images of conductive silver ink.....	35
4.4 (A) Conductive silver ink was demonstrated for conductive pen, (B) stamp printing, and (C) electric circuits were printed by drop-on-demand printer.....	36
4.5 Silver citrate complex at various concentration of starch solution, (A) no starch, (B) 0.1 % (w/v), (C) 0.25 % (w/v), and (D) 0.50 % (w/v). Each picture, the bottles on the left hand side to right hand side are silver citrate complex that had molar ratio of trisodium citrate dihydrate to silver nitrate, $[\text{trisodium citrate}]/[\text{AgNO}_3]$ from 4.0×10^{-3} , 8.0×10^{-3} , 1.6×10^{-3} , and 3.2×10^{-3} , respectively.....	37
4.6 The photographic images of (A) Silver citrate complex that had $[\text{trisodium citrate}]/[\text{AgNO}_3]$ from 4.0×10^{-3} , 8.0×10^{-3} , 1.6×10^{-3} , and 3.2×10^{-3} , respectively and (B) silver nanoparticles were synthesized from silver citrate complex with NaBH_4	38

Figure	Page
4.7 AFM images of silver particles at various [trisodium citrate]/[AgNO ₃], (A) No citrate, (B) 4.0×10 ⁻³ , (C) 8.0×10 ⁻³ , and (D) 1.6×10 ⁻³ . Silver nanoparticles size in the range of 30-60, 5-30 nm, 30-50 nm, and 30-80 nm, respectively.....	38
4.8 Schematic diagram of mechanism for formation of silver nanoparticles without trisodium citrate.....	39
4.9 Schematic diagram of formation of silver nanoparticles mechanism with [trisodium citrate]/[AgNO ₃] equal to (A) 4.0×10 ⁻³ and (B) 8.0×10 ⁻³ before redox reaction occurred.....	40
4.10 AFM images of silver nanoparticles at (A) 1 ppm, (B) 10 ppm, (C) 100 ppm, (D) 1,000 ppm, (E) 10,000 ppm, and (F) 100,000 ppm concentrations.....	43
4.11 AFM images of silver nanoparticles at (A) 10,000 ppm and (B) 100,000 ppm concentrations.....	44
4.12 (A) AFM image of silver nanoparticles at 100,000 ppm concentration after sintering. (B) Phase image of Figure 4.12A. Type I and Type II represented the type of sintering mechanisms....	45
4.13 AFM images of silver nanoparticles after sintering at various condition; (A) room temperature, (B) 100 °C, for 10 min., (C) 200 °C, for 120 min., and (D) mechanical rubbing.....	46

LIST OF TABLES

Table	Page
4.1 Condition in silver nanoparticles synthesized by chemical reductive method.....	32
4.2 Sheet resistivity of silver particles after sintering at various conditions.....	47



ศูนย์วิทยทรัพยากร
จุฬาลงกรณ์มหาวิทยาลัย

LIST OF ABBREVIATIONS

AgNO ₃	: silver nitrate
NaBH ₄	: sodium borohydride
LSPR	: localized surface plasmon resonance
DDA	: discrete dipole approximation
nm	: nanometer
Ag	: Argentum (silver)
eV	: electron volt
TEM	: transmission electron microscopy
AFM	: atomic force microscopy
ATR FT-IR	: attenuated total reflection Fourier transform infrared



ศูนย์วิจัยทรัพยากร
จุฬาลงกรณ์มหาวิทยาลัย

LIST OF SYMBOLS

Ω	: Ohm
$^{\circ}\text{C}$: degree Celsius
E	: redox potential
E_{redox}	: solution potential
M	: metal



ศูนย์วิทยทรัพยากร
จุฬาลงกรณ์มหาวิทยาลัย

CHAPTER I

INTRODUCTION

1.1 Conductive ink made of silver nanoparticles.

Conductive ink made of silver nanoparticles was formerly designed for writing and repairing electrical circuit. Nowadays, it could also be applied for fabricating electrical circuit by ink-jet printing [1-5]. Mostly, conductive silver ink was made from silver powder by digestion of silver metal with physical technique such as milling and spray pyrolysis. Silver powder was then mixed with binder (e.g. hydrocarbon compound and/or polymer) and employed as conductive silver ink. However, silver content of conductive ink was more than 60-80 % (w/v) because when it dried on a substrate, silver particles could be contacted and became a conductive silver line [6-8].

Recently, conductive silver ink was developed from silver nanoparticles with less amount of silver load and it could be used to fabricate very fine conductive pattern and a thermal sensitive substrate [8-9]. Generally, high concentration of silver nanoparticles could not show conductive property because the stabilizer protect against aggregation in nanoparticles. Silver nanoparticles were shown conductive property after stabilizer was decomposed by thermal treatment thus the silver particles were then sintered together. However, sintering phenomenon in silver nanoparticles depended on the size of particles [10-11]. Smaller size of silver particles led to lower sintering temperature. The sintering phenomenon enhanced conductivity because particles as the contact among particles were increased.

In this work, method for synthesizing high concentration of silver nanoparticles that had the lowest concentration of stabilizer for using as conductive silver ink were developed. When silver particles were in the colloid form, silver nanoparticles were stabilized by stabilizer. The silver ink became conductive after deposition and drying on substrate. Furthermore, in this method, the particles size was controlled by stabilizer at various concentrations. When silver particles were small enough, sintering phenomenon occurred at ambient temperature. This conductive silver ink was employed for making the conductive line by stamp printing, screen printing, drop-on-demand printing and using as conductive pen.

1.2 The objectives

The objectives of this research is to develop new methods for synthesizing small silver nanoparticles for the applications as conductive silver ink.

1.3 Scopes of research

1. Developing a novel method for synthesizing silver nanoparticles as conductive silver ink.
2. Investigating the effects of stabilizer concentration on the size of synthesized silver nanoparticles.
3. Analyzing the influence of concentration of silver nanoparticles on the sintering phenomenon at room temperature.
4. Examining the relationship between morphology and resistivity of silver film at different heat-treatment temperatures and heat-treatment times.

CHAPTER II

THEORETICAL BACKGROUND

2.1 Silver nanoparticles

Silver nanoparticles are of great interests in scientific research and industrial application, due to the large surface area to volume ratio and size-dependent properties. Silver nanoparticles have been used in many applications in different area of science such as catalysis [12], surface enhance vibration [13], optical sensor [14-15], antibacterial agent [16-17], and conductive material [8-10].

Noble metal nanoparticles (especially gold, silver, and copper) exhibit a strong UV-visible absorption band that is not present in the spectrum of the bulk metal. This absorption band results when the incident photon frequency is resonant with the collective oscillation of the conduction electrons and is known as the *localized surface plasmon resonance* (LSPR) [19]. When the environment of metal nanoparticles was changed, LSPR shifts were observed. Electromagnetic field enhancement near the surface of nanoparticles is associated with extinction efficiency of nanoparticles, responsible for the intense signals.

Furthermore, size of silver nanoparticles affects the melting temperature or sintering temperature. Sintering effect occurs through diffusion of elements across particles, forming interconnection (necking) between particles. This phenomenon always occurs at high temperature. However, sintering can occur at room temperature when particles size is reduced to nanoscale. Therefore, silver nanoparticles could be employed as conductive ink or conductive paste for electronic circuit fabrication.

Then, the developments of synthesis methods for silver nanoparticles have been explored in order to control size and shape of particles [20-21]. There are many methods to synthesis silver nanoparticles. In general, the synthesis methods are classified into two approaches, “bottom-up” and “top-down” approaches. Bottom-up approach is getting started with the atom or molecule for building up the desired nano-objects. Top-down approach, standard bulk material can be broken up and produced the same materials in the form of nanometric grains.

2.2 Size effect in nanochemistry

The size effect in nanochemistry create a phenomenon that produces the qualitative changing in physical, optical, and thermal properties based on the number of atom or molecules at the surface of nanoparticles and takes place in the range of 1-100 nm. Each new property enables new applications.

2.2.1 Physical property

Physical properties, such as hardness, are dependent on the arranged structure of material and/or defects within a material. For size decreasing system, the arrangement and defection in the structure become changing so that nanoparticles have a very high surface to volume ratio. In addition, the high surface to volume ratio in nanostructure leads to enhanced properties in catalytic materials and antibacterial materials.

2.2.2 Optical property

In metal nanoparticles, the optical property is associated with unusual electron energy level arranged in a discrete fashion. For bulk metal, the energy level merges and leading to continuous adsorption. The decrease in particles size increased the energy gap which leads to discrete-like energy level of absorption.

The interaction between electrons around the particles and photons are resulted in electronic and/or vibration excitation. The collective excitation leads to the oscillating of delocalized conduction electrons. The excitation of conduction electrons is conventionally considered as a surface plasmon. When the photon frequency resonates with the oscillation of conduction electron in the metal nanoparticles, the frequency is called the Localized Surface Plasmon Resonance (LSPR) frequency. The LSPR depends on size, shape, and composition of particles interparticles spacing and dielectric properties of the surrounding media. The optical properties in metal nanoparticles are much more complicated. The extinction intensity of nanoparticles consists of two parts: absorption and scattering intensity. For spherical particles, extinction intensity can be calculated by Mie's theory [22]. For other shapes or arbitrary shapes, the discrete dipole approximation (DDA) were employed. The DDA is a finite-element method that approximates a continuum target by a finite of polarizable point [20, 23-24].

2.2.3 Thermal property: melting point

The melting temperature depression due to the high surface area to volume ratio in nanoparticles is significant when the particles size become very small. The dependence of the melting point on the metal particle size was considered within the two models, thermodynamic consideration and atomic vibration consideration [25].

1. Thermodynamic consideration

This argument is not only predict chances of the melting point for small particles but also help us to understand the process of the surface melting. The transition from solid to liquid as the temperature increased will start at the surface of the particles while the internal core still preserve as a solid. This surface melting is due to the surface tension at the solid-liquid interface affecting the energy balance of the system. Supposed that a small solid spherical particle with radius, r , is at thermal equilibrium with surrounding liquid shell. The infinitesimally small outer layer of the solid particles melts such that a mass dw of the material change from solid

to liquid phase. The change in the mass of particle and its size will result in an infinitesimally small reduction of the particles surface area, dA . The relationship between dw and dA in spherical particles are as follows:

$$\frac{dA}{dw} = \frac{2}{\rho r} \quad (2.1)$$

where ρ is the density of material and r is radius at equilibrium. The energy balance associated with this change can be shown as follows:

$$\Delta U dw - \Delta S \theta_r dw - \sigma dA = 0 \quad (2.2)$$

where ΔU is the change of internal energy and ΔS is the change of entropy per unit mass of a metal during melting, σ is the surface tension coefficient for a liquid-solid interface, and θ_r is the melting temperature of small particles. In case of bulk material, it does not contain the surface tension term:

$$\Delta U dw - \Delta S T_m(\infty) dw = 0 \quad (2.3)$$

$$\Delta S = \frac{\Delta U}{T_m(\infty)} = \frac{L}{T_m(\infty)} \quad (2.4)$$

where $T_m(\infty)$ is the melting temperature of bulk material, L is the latent heat of fusion, and ΔU and ΔS are independent of temperature. From equations 2.1, 2.2, and 2.4, the melting temperature can be derived:

$$\Delta\theta = T_m(\infty) - \theta_r = \frac{2T_m(\infty)\sigma}{\rho L r} \quad (2.5)$$

In case of gold nanoparticles when the size of gold is approximately 1 nm, the melting temperature is about 900 K which lowers than its bulk value (1,337.33 K).

2. Atomic vibration consideration

The melting behavior of small particles can be understood in terms of the Lindemann criterion [25]. The criterion indicates that the crystal will melt when the root-mean-square displacement of the atom in crystal, δ , exceeds a certain fraction of interatomic distance a :

$$\frac{\delta}{a} \geq \text{const.} \quad (2.6)$$

The increase in temperature will increase the amplitude of oscillation of atoms at the surface. When the oscillation is strong enough, the crystal structure of solid and melting occurs. Surface atoms are not strongly bound, the amplitude of vibration at given temperature is higher than that of atom within the volume of the particles. This effect can be described by the ratio of mean-square atom displacement on the surface, δ_s and inside of the particles δ_v :

$$\alpha = \frac{\delta_s}{\delta_v} \quad (2.7)$$

A model that considered the decrease in the nanoparticles melting temperature with a decrease in the size, was developed [27]. The following equation was proposed for the description of nanoparticles properties:

$$\frac{T_m(r)}{T_m(\infty)} = \exp \left[-(\alpha - 1) \left(\frac{r}{3h} - 1 \right)^{-1} \right] \quad (2.8)$$

where $T_m(r)$ is the melting temperature of the nanocrystal, $T_m(\infty)$ is the melting temperature of the bulk material, and h is the height of a monolayer of atoms in its crystal structure. This equation can be used to predict the melting point of

nanoparticles if the α is known. In case of nanoparticles the α is adjusted to fit the experimental data.

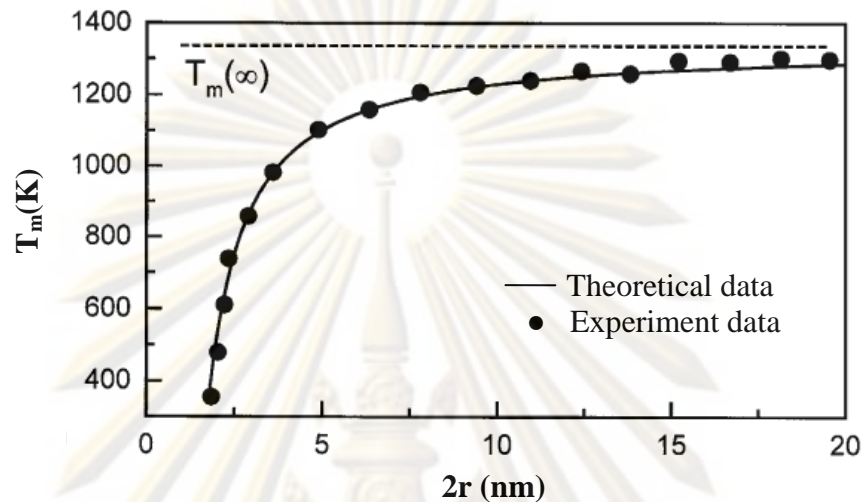
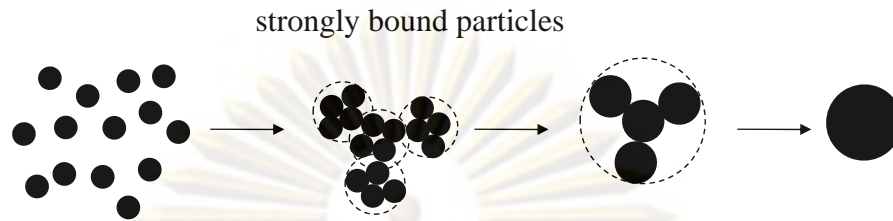


Figure 2.1 Dependence of gold nanoparticles base on atomic vibration consideration [27]

2.3 Sintering phenomenon

The sintering process is an irreversible thermodynamic phenomenon which changes unstable aggregates of primary particles with excess free energy into compact particles with a stable structure. Generally, the sintering mechanisms can be divided into two mechanisms depending on the strength of bonds between the primary particles (Figure 2.2). With strongly bound particles (Figure 2.2 A), coalescence is the main mechanism and the primary particles subsequently fuse together to finally form a compact particles. In case of weakly bound particles, the aggregates compact by the rearrangement of primary particles, Figure 2.2 B. For the final step, the constituents of the aggregate may coalesce to form fully compacted particles. In the real systems, the sintering process may be the combination of these two mechanisms [28-29].

A: Surface area change mechanism:



B: Rearrangement mechanism:

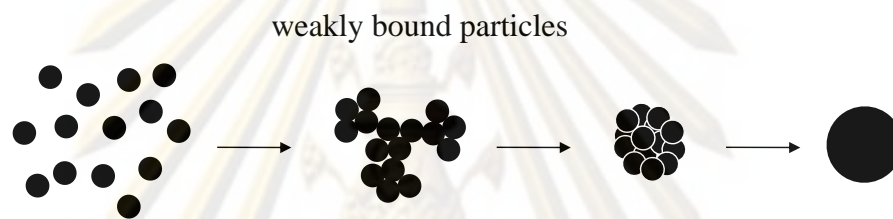


Figure 2.2 Schematic diagram of sintering mechanism of particles: (A) surface area change mechanism and (B) rearrangement mechanism.

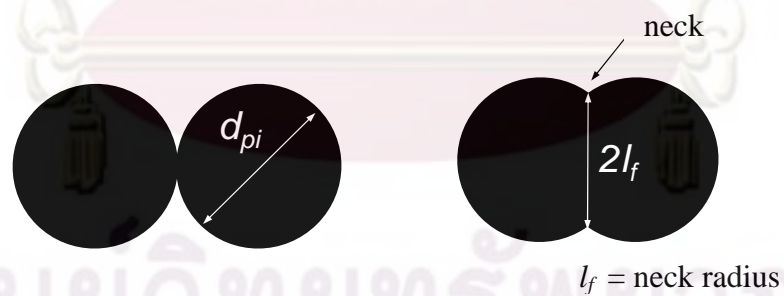


Figure 2.3 Schematic diagram of sintering process between two spherical particles.

1. Surface area change mechanism

The surface area change caused by sintering is given by the following equation:

$$\frac{da_s}{dt} = -\frac{1}{\tau}(a_s - a_{sc}) \quad (2.9)$$

where a_s and a_{sc} are the surface area of the agglomerate at time t and that of the completely compacted agglomerate, respectively.

The sintering time, τ , is the time at which two equally sized spheres coalesce, when the neck radius l_f reach 0.83 of the value of the radius, $d_{pi}/2$ of the primary particles (Figure 2.3). The sintering time is given by the following equation:

$$\tau = (2l_f / d_{pi0})^n d_{pi}^m / K = Ad_{pi}^m \exp(E / R_g T) \quad (2.10)$$

The solid phase diffusion, A and E represent the diffusion coefficient depending on the sintering mechanism and the activation energy, respectively. The parameters m and n are depending on the sintering mechanism. For the grain boundary diffusion model, the parameters m and n are 4 and 6, respectively [29]. The d_{pi0} is an initial value.

$$A = \frac{\kappa T (2l_f / d_{pi0})^6}{400bD_0\gamma\Omega} \quad (2.11)$$

where b , D_0 , γ , and Ω are the width of gain boundary, the pre-exponential factor for diffusion coefficient, the surface tension, and the atomic volume, respectively.

$$d_{pi} = 6V / a_s \quad (2.12)$$

where $a_s (\pi d_{pi}^2 N)$ is the surface area of agglomerate particles, $V(\pi d_{pi}^3 N / 6)$ is the volume of agglomerate particles and N is the total number of primary particles.

The essential assumptions needed to carry out the calculation including:

1. The primary particles are monodisperse and spherical.
 2. The mass and the volume of an aggregate are preserved throughout the process.
 3. The coordination number and the geometric shape remain constant during sintering, except for the final step, fractal particle merges into homogeneous spherical particles.
2. The rearrangement mechanism

The particles are dispersed with weak interaction between the particles. This state is called the *dispersed state*, and the Gibbs free energy of the particles is at its maximum and the coordination number is assumed zero. The dispersion particles in dispersed state are closely packed to condensation state and coordination number is greater than one. The driving force for the rearrangement process can be expressed as follows:

$$\frac{dc_N}{dt} = -L(c_N - c_{Neq}) \quad (2.13)$$

where c_N is the coordination number, c_{Neq} is the coordination number in the equilibrium state (lowest Gibbs free energy) and L is the rate coefficient for restructuring.

The Gibbs free energy per primary particles can be related to coordination number by the following equation:

$$G = (1/2)\varepsilon_B c_N \quad (2.14)$$

where ε_B is the average bond energy between two primary particles that prevent rearrangement.

In this analysis, the value of c_N was related to measurable agglomerate parameter, the fractal dimension D_f defined by the following equation:

$$N = A \left(\frac{d_p}{d_0} \right)^{D_f} \quad (2.15)$$

where N is the average number of primary particles per agglomerate, A is the proportionality constant, d_0 is the diameter of primary particles, d_p is the diameter of agglomerate and D_f is the fractal dimension. Then, c_n is defined by the following equation:

$$c_n = N - 1 = AB^{D_f} - 1 \quad (2.16)$$

Further essential assumptions needed to carry out the calculation up to now is twofold:

1. The primary particles are monodisperse and spherical
2. The number and the diameter of the primary particles of agglomerate do not change during the rearrangement.

Effect of sintering on resistivity

The change in resistance arises from sintering, a material transport process based on the atomic diffusion driven by reduction of surface energy [10]. The schematic diagram of possible diffusion step during sintering between two particles is shown in Figure 2.4. Step 1 and 2 are lattice and surface diffusion mechanisms, respectively. These mechanisms maintain the distance between centers of particles.

In step 3 and 4, the atoms are moved from the contact surface and the center of the spheres can move toward one another. The neck formation is also driven by the reduction in surface energy by atomic diffusion. As a result, particles contact area increased.



Figure 2.4 Schematic diagram of diffusion step between two particles, step 1 and 2 are lattice and surface diffusion mechanisms, respectively. These two steps do not produce any shrinkage. Step 3 and 4 are densification, center of particles approach to one another. These two steps are through-lattice diffusion and grain boundary diffusion.

The resistivity based on the geometry— the two-sphere sintering model was introduced by Frenkel [30]:

$$L(t) = L(0) \times \sqrt{1 - \left(\frac{z}{r}\right)^2} \quad (2.17)$$

where $L(0) = 2a$ and the fractional neck radius is z/r . The resistivity was related to the shrinkage on aggregation of two spherical particles, based on two assumptions.

1. The linear contraction in vertical dimension is equal to the decrease in the distance between the sphere centers.
2. The atomic diffusion path maintains shape as the spheres approach each other.

The above assumptions result in the following relation between resistance and resistivity:

$$R = \rho_0 \int_{-a}^a \frac{dx}{A} = \rho_0 \frac{1}{r^2} \int_{-a}^a \frac{dx}{\pi(z/r)^2} \quad (2.18)$$

where ρ_0 is the initial resistivity of the material, x is the distance along the centerline of two spheres, and A is the contact area between the spheres. The completely sintered can be geometrically represented $2r$. The resistivity can be expressed in terms of the linear distance L . Thus, $\rho(t)$ as the function of time was defined by the following equation:

$$\rho(t) = \frac{2\rho_0}{\pi} \times \ln \left\{ \frac{r + L(t)/2}{r - L(t)/2} \right\} \quad (2.19)$$

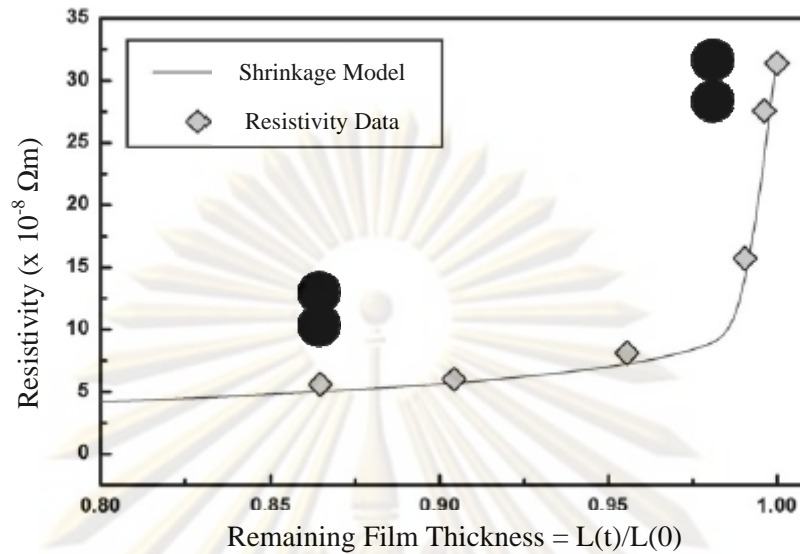


Figure 2.5 Resistivity as a function of linear shrinkage at 150 °C predicted by the shrinkage model versus experimental data [10].

2.4 Synthesis of silver nanoparticles

Generally, all methods for synthesis of nanoparticles can be divided into two main types, *bottom-up* and *top-down* approaches. In the bottom-up approach, getting started with the atom or molecule and built up nanoparticles. In top-down approach is getting started from standard bulk materials to generate nanomaterial. However, methods of synthesis metal nanoparticles synthesis method have two important aspects, chemical method and physical method.

Chemical reduction

Chemical reduction is widely used in liquid phase, including aqueous and nonaqueous media. The metal nanoparticles were synthesized by chemical reduction of metal salt with a reducing agent (e.g. borohydrides, formaldehyde, alcohol, and carboxylic compound). Generally, the behavior of metal particles in solution is determined by the potential difference [31-38]:

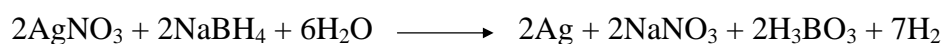
$$\Delta E = E - E_{redox}$$

where E is the equilibrium redox potential of the particles and E_{redox} is the corresponding solution potential. When $\Delta E > 0$, the particles are being. When $\Delta E < 0$, the particles are dissolved. This becomes more complication by the fact that the redox potential of metal particles depends on the number of atoms. Chemical interactions in the reduced metal ion system can be associated with the transfer of an electron from the reducer to metal ion via the formation of an intermediate complex. Furthermore, the chemical reduction is multifactor process. The concentration of its components, temperature, and pH of medium are also induced for consideration.

The common reagents used in reduction of metal ions are tetrahydroborate of alkali metal (MBH_4). Alkali-metal tetraborates can reduce many cations of transition and heavy metals, because the high redox potential of MBH_4 .

Borohydride reduction

Tetrahydroborate of alkali metal ion (MBH_4) has been frequently used as reducing agent for synthesis of metal nanoparticles in aqueous media [36-38]. Borohydrides reduce metal ions with high reduction potential, 1.24 V in alkaline solution compared with the standard potential of the metal ion, 0.5-1.0 V. The reactions of borohydrides occur rapidly causing the immediate nucleation of metal particles. The obtained metal particles from borohydride reduction are small and have a narrow size distribution. Chemical interaction associated with the transfer of an electron from the reducing agent to metal ion via the formation of $M \cdots H \cdots B$ complex, which lowered the electron-transfer energy. However, it is difficult to control the reaction to obtain the larger particles. In addition, borohydride was considered as a toxic reducing agent. The metal particles obtained by borohydride reduction were not suitable for the medical application, otherwise they have to be purified before using. The redox reaction can be written as follows [34]:



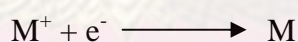
Photochemical and radiation-chemical reduction

Synthesis of metal nanoparticles by photochemical (photolysis) and radiation-chemical (radiolysis) processes was associated with the generation of high active reducing agent such as electrons, radicals and excited species [39-40]. These two methods are different in energy that applied to the process. Photochemical involves energies below 60 eV, but radiation-chemical requires energies of 103-104 eV. These methods have many advantages such as the absence of impurities, resulting in high purity nanoparticles and nanoparticles can be produced at low temperature.

Photochemical reduction in solution is widely used in synthesis metal nanoparticles synthesis. The particles are obtained from metal salt solution in water, alcohols, and organic solvent. Under the action of light, the active species are formed:



A solvated electron interacts with metal ion producing metal particles:



For radiation chemical reduction, atoms and small metal cluster are formed, which is followed by their transformation into nanoparticles. The metal nanoparticles in solution can be stabilized in the medium solution or by addition stabilizer after synthesis. Photochemistry and radiochemistry are available and reproducible. The narrower size distribution of particles was obtained.

Physical method

There are many different physical methods for preparation of metal nanoparticles. The major method is the process based on combining metal evaporation into an inner gas flow with subsequent condensation in a chamber maintained at certain temperature. Physical fabrication methods of metal nanoparticles employ inert gas condensation [41], laser ablation [42], spray pyrolysis [43].

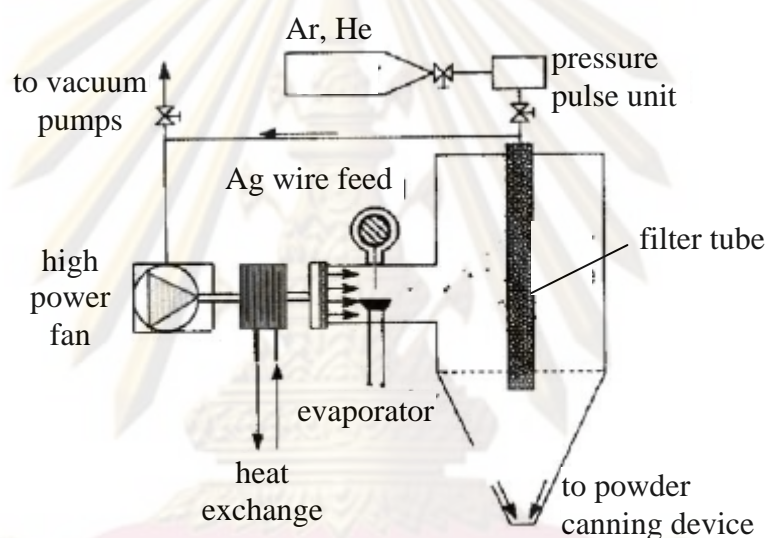


Figure 2.6 Schematic diagram for the preparation of silver nanoparticles by inert gas condensation (IGC) method. The pure inert gas (He or Ar) flows into the chamber and the source metal is vaporized into the flowing inert gas. As a result, nanoparticles are formed on suitable medium such as metal filter.

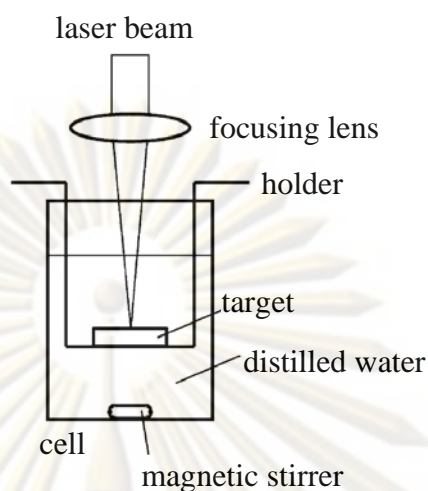


Figure 2.7 Schematic diagram for experimental set-up for colloid preparation by laser ablation in solution. Metal nanoparticles can be produced by irradiating metal sheet with intense laser in liquid solution with the present of stabilizer. Interaction between laser and metal sheet resulted in ablation. The particles size can be controlled by changing the laser intensity and wavelength.

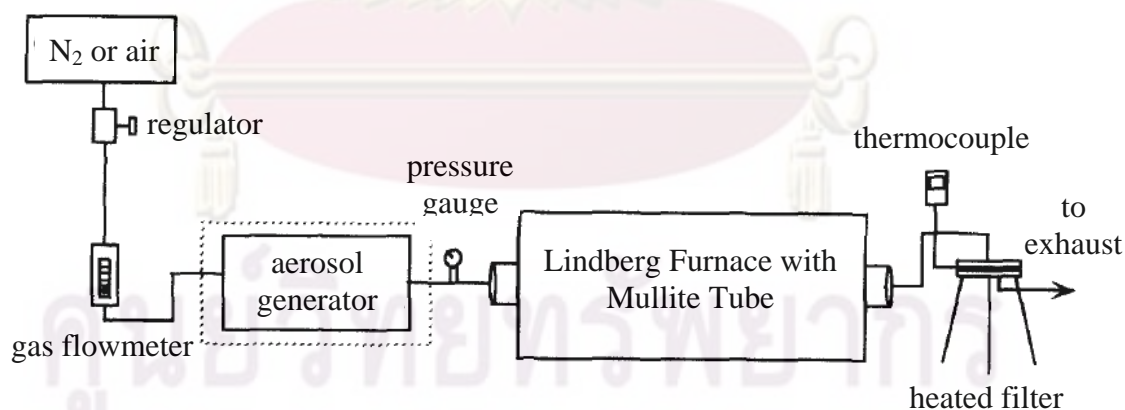


Figure 2.8 Schematic diagram for experimental setup of spray pyrolysis. The metal salt solution is atomized into droplets and sent through a hot reactor. Then, the metal salts decompose to form the particles.

Stabilizer

Metal nanoparticles are small enough to be pushed around by the molecular collision of the surrounding media, this effect called *Brownian motion*. The Brownian motion is a random motion, collision of particles was occurred leading to aggregation of particles. Surface protection mechanisms were developed to maintain the stability of nanoparticles. In general, there are electrostatic stabilization and steric hindrance mechanism. Electrostatic stabilization mechanism is involving the adsorbed ions on the surface of the particles and the counter ions around the particles. The sufficient electrostatic repulsion can prevent their agglomeration. Steric hindrance mechanism can be achieved by the adsorption of large molecules such as polymers on the surface of metal nanoparticles. Polymer chains between approaching particles results in steric repulsion which separate the particles.

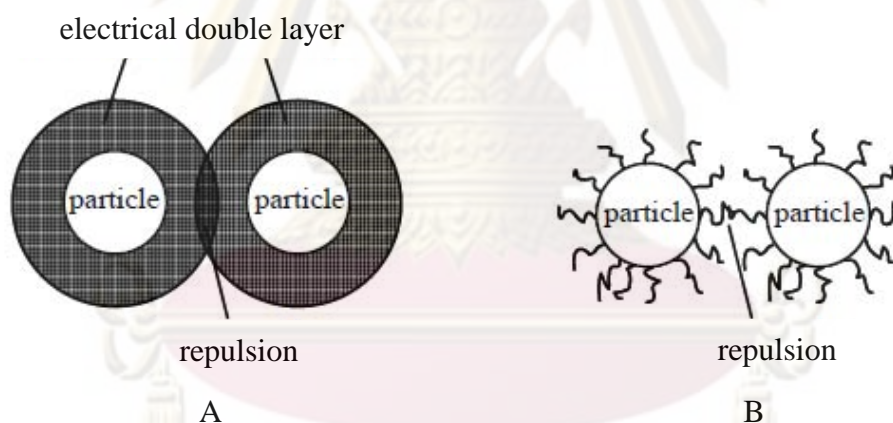


Figure 2.9 Schematic diagrams of (A) electrostatic stabilization and (B) steric hindrance.

2.5 Silver nanoparticles as conductive ink

There are three important factors that have critical impacts on the using silver nanoparticles as conductive silver ink.

The first factor is the conductivity of silver metal itself. In case of silver nanoparticles, this high conductivity is also maintained.

The second factor is silver nanoparticles must have the optimal concentration (more than 10-30 % wt). When the silver particles were dried on a substrate and the solvent were evaporated, closely pack of silver particles were observed. Then, electrical conductivity was allowed by high silver load. At low silver load, insulation layer (e.g. stabilizer, polymer) was prevalent, which reduced resistance between silver particles.

The last factor is the size of particles. The decrease in size of silver particles is the decrease in melting temperature. These will lead to decrease in the surface premelting or sintering temperature. The lower sintering temperature or melting temperature is a result of high surface area to volume ratio in nanoparticles. Although, a direct contact between the silver nanoparticles can be accomplished, a contact resistance at interface is still present. The sintering between particles can minimize the resistance because reduction in total interface area. Relation between sintering phenomenon and conductive property were intensively described in section 2.3.

ศูนย์วิทยทรัพยากร

จุฬาลงกรณ์มหาวิทยาลัย

2.6 Characterization techniques

2.6.1 Atomic force microscopy

The atomic force microscope (AFM) uses a laser beam deflection system which is reflected from the back of the reflective AFM cantilever onto a position-sensitive photodetector. AFM tips and cantilevers are fabricated from silicon (Si) or silicon nitride (Si_3N_4). Typical tip radius is 1-10 nanometers. When the tip is brought into a sample surface, force between the tip and the sample lead to deflection of the cantilever according to Hooke's law. The force such as, van der Waals forces, electrostatic force, magnetic forces, capillary force are measured by AFM.

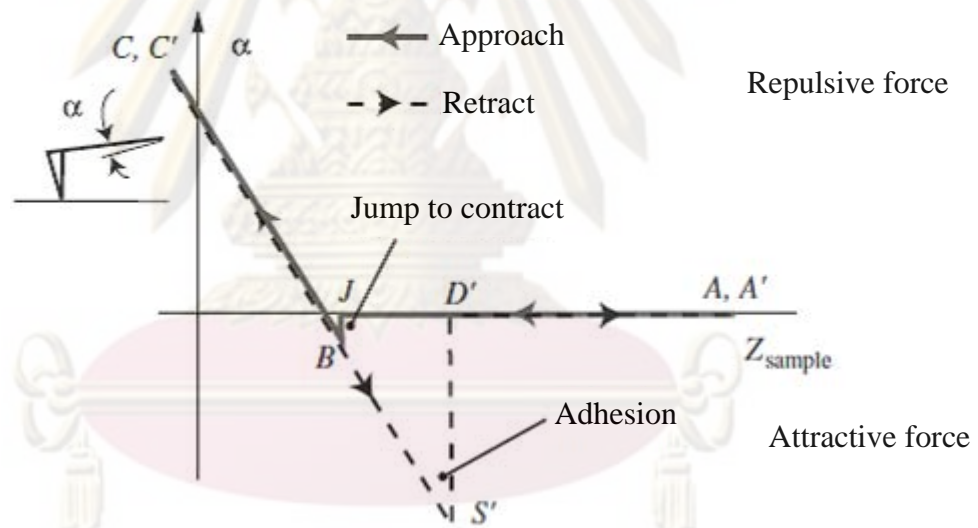


Figure 2.10 Schematic diagram of force curve on an ideal non-deformable material. The deflection of the cantilever is a function of the vertical position of the sample during an approach-retract cycle.

A laser beam is focused on the back of the cantilever and reflects into four-quadrant photodetector. Normal forces deflect the cantilever up or down, lateral forces twist the cantilever left and right. These deflections are simultaneously and independently measured by monitoring the deflection of the reflected laser beam.

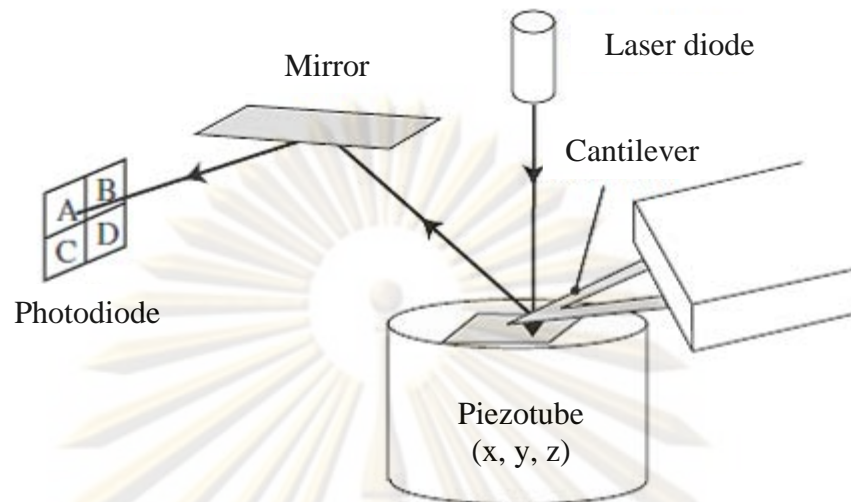


Figure 2.11 Schematic diagram of the atomic force microscope [44].

The method for measuring interaction between sample surface and AFM tip can be derived into two main methods, *contact mode* and *non-contact mode*. In contact mode the tip scans the sample in close contact with the surface. The force on the tip is attractive or repulsive between 10^{-9} - 10^{-6} N. The deflection of the cantilever is sensed leading to deflection of laser beam on photodiode. If the measured deflection is different from the desired value, the feedback amplifier will apply a voltage of piezo to raise or lower the sample relative to the cantilever to restore the desired value of deflection. The voltage that the feedback amplifier applies to the piezo is the measure of the height of features on the sample surface. The main problems of the contact mode are damaging technique both probe and sample surface.

In non-contact mode, the tip is positioned above the surface sample in the range of 50 - 150 angstrom. Attractive van der Waals forces acting between the tip and the samples are detected, and the topographic images are constructed by scanning the tip above the surfaces. However, the attractive forces from non-contact mode are weaker than the force that can be measured by contact mode. Thus, the tip must be given small oscillation by electrical circuit, this method can be detected the small force between the tip and the sample by measuring the change of amplitude, phase, or frequency of the oscillating cantilever in response to force gradients from the sample.

Topography and homogeneity in the sample surface can be observed by AFM. A tip approach into the sample surface, the probe oscillates vertically near its mechanical resonance frequency. When probe taps lightly on the surface, the amplitude of oscillation is reduced and the AFM uses amplitude changing to observe the surface topography. In addition, the probe motion can characterize phase change when the probe encounters different composition region. Phase images often show extraordinary contrast for many composition surfaces such as the closely packs of particles, grain boundary, which were no distinguished by topographic image.

2.6.2 Transmission electron microscopy

Transmission electron microscopy (TEM) was widely used for studying the size, size distribution and morphology of particles. TEM involves a beam of accelerated electron with energy of 50-200 keV emitted by a cathode in vacuum. These electrons are deflected in small angles by atoms in sample and transmitted through thin sample. Then, these electrons are magnified by magnetic lenses and hitting a fluorescent screen generating the bright field image. Schematic diagram of transmission electron microscope is shown in Figure 2.17. The interactions of electron beam with atoms in the samples are the diffraction or absorption of electron beam. The images from electron microscopes indicate the structure of a sample which can be used for determining size and morphology of metal nanoparticles.

ศูนย์วิทยทรัพยากร

จุฬาลงกรณ์มหาวิทยาลัย

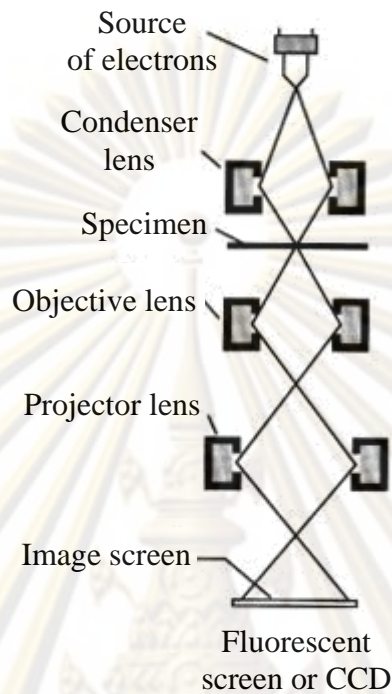


Figure 2.12 Schematic diagram of transmission electron microscope (TEM)

2.6.3 Four-point probe measurement

The apparatus used to measure the sheet resistivity is the Four-point probe [45]. By passing a current through two outer probes, a voltage is induced in the inner voltage probes. If the sample has any resistance to the flow of electrical current, this will result in a drop in potential.

ศูนย์วิทยทรัพยากร
จุฬาลงกรณ์มหาวิทยาลัย

2.6.4 Attenuated Total Reflection Fourier Transform Infrared (ATR FT-IR) spectroscopy

ATR FT-IR spectroscopy is the characterization technique based on an internal reflection phenomenon. The radiation travels in a higher refractive index material impinges on the interface with a less dense medium. When incident angle is greater than critical angle, the incident radiation is completely reflected. In addition, there is an electromagnetic field that extends beyond the crystal surface, it is called *evanescent wave*. If an absorbing material is contacted with internal reflection element (IRE), the evanescent wave will absorb at wavelength where the material has an absorption band. The amount of energy reflected back through the IRE will be attenuated. This technique is called *Attenuated Total Reflection*.

For ATR technique, the reflectivity is a measurement of the interaction of the electric field with the material. The resulting spectrum is also a characteristic of the material. The molecular information and chemical composition can be obtained.

2.6.5 UV-Visible spectroscopy

UV-Visible spectroscopy is widely used to determine the optical properties of material in solution phase. Light is traveling through the sample and the amount of transmitted light is measured. The absorption in the UV-Visible range directly affects the color of material, undergoing electronic transition. However, in case of metal nanoparticles, the optical properties are much more complicated. The measured absorbance spectrum is the extinction of the light, which is the summation of absorption and scattering intensity of nanoparticles. Extinction and absorption intensity of spherical particles of arbitrary size can be calculated by Mie's theory.

CHAPTER III

EXPERIMENT

3.1 Chemicals and materials

- 3.2.1 Silver metal 99.99%
- 3.2.2 Nitric acid (Merck)
- 3.2.3 Acetone (Merck)
- 3.2.4 Sodium borohydride (Merck)
- 3.2.5 Trisodium citrate dihydrate (Baker Analyzed reagent)
- 3.2.6 Soluble starch (Merck)

3.2 Silver nanoparticles synthesis method for conductive ink.

Silver nitrate (AgNO_3) solution was prepared by dissolving 6.32 g of silver nitrate in 100 mL 0.1 % (w/v) of soluble starch solution. Sodium borohydride (NaBH_4) was used as a reducing agent. The molar concentration ratio of the reducing agent to silver nitrate was adjusted to 0.7, 0.9 and 1.0 to investigate the optimum ratio for synthesized silver nanoparticles. In this work, trisodium citrate dihydrate was used as the stabilizer. Both reducing agent and stabilizer were dissolved in 0.1 % (w/v) of soluble starch solution. The redox reaction occurred in the reactor (three-ways connection tube).

An apparatus for synthesis of silver nanoparticles was shown in Figure 3.1. Early in the reaction, trisodium citrate solution was added into the silver nitrate solution, and silver citrate complex were formed. After that, silver citrate complex and sodium borohydride solution were loaded into the syringe which connected with reactor. Silver citrate complex and sodium borohydride solution were injected

into reactor and the redox interaction occurred. Small sizes of silver nanoparticles were obtained.

After reaction, the supernatant was separated by centrifugation and silver nanoparticles were repeatedly washed with distilled water. The silver nanoparticles were redispersed in the 0.1 % (w/v) of trisodium citrate solution. After ultrasonic, the conductive silver ink was yielded. Particles sizes, size distribution, and morphology of silver particles were observed by transmission electron microscope (TEM) and atomic force microscope (AFM). The supernatant and washing solution were investigated with UV-Visible spectroscopy and ATR FT-IR microspectroscopy. The result suggested the residual compositions such as silver ion residual and borate compound.



Figure 3.1 Apparatus for synthesis of conductive silver ink.

3.3 The effect of stabilizer concentration on the size of silver nanoparticles.

Size, size distribution, and morphology of silver nanoparticles were depended on the various reaction conditions. In the present work, the concentration of trisodium citrate and the concentration of soluble starch were investigated.

The mole ratio of trisodium citrate to silver nitrate was varied from 4.0×10^{-3} , 8.0×10^{-3} , 1.6×10^{-2} to 3.2×10^{-2} . The mole ratio of the reducing agent to silver nitrate was maintained at 1.0. And in this reaction, soluble starch 0.10, 0.25, and 0.50 % (w/v) were used as solvent. The size, size distribution, and morphology were investigated by AFM.

3.4 Sintering phenomenon of conductive ink made of silver nanoparticles.

The sintering phenomenon of conductive silver ink was investigated at various concentrations of silver particles which in the range of 1-100,000 ppm. The conductive silver ink at concentration 100,000 ppm was synthesized and diluted to the desired concentrations. The investigation sintering temperatures were at room temperature, 100 °C for 10 min, and 200 °C for 120 min. The effect of mechanical rubbing was also investigated. The morphology changes of silver nanoparticles were observed by AFM. The sheet resistivity of each condition was measured with four-point probe. Correlation between morphology change on silver films and resistivity were investigated.

3.5 Characterization of synthesized conductive silver ink.

3.5.1 Atomic force microscope

Atomic force microscope (AFM) for the observation of silver nanoparticles was commercial SPA-400 atomic force microscope (Seiko Instrument, Inc., Japan) with a calibrated 20 micrometer XY-scan and 10 micrometer Z-scan range PZT-scanner. AFM measurement was carried out in non-contact mode using silicon tips with a force constant of 13 N/m and resonance frequency is 132 KHz in ambient air. All reported images were scanned with scan rates in the range of 0.5-1.0 Hz.

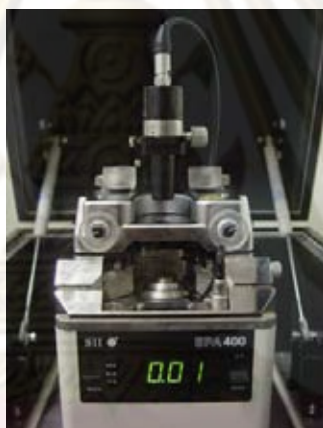


Figure 3.2 Probing station of the Seiko SPA-400 atomic force microscope

3.5.2 Transmission electron microscope (TEM)

A Transmission electron microscope (TEM) image of conductive silver inks were recorded with a Hitachi, H-7650 analytical transmission electron microscope. Samples were prepared by placing a drop of silver nanoparticles solution onto a carbon-coated copper grid or formvar-coat copper grid. After the solutions were dried, size and size distribution of silver nanoparticles in conductive silver inks were observed. The accelerating voltages of this instrument are in the range of 40 - 120 kV and image magnifications are in the range of 1,000-40,000 times.

3.5.3 Resistivity measurement technique

In this study, sheet resistivities were measured with four-point probe measurement. Conductive silver inks were dropped on cover glass slides and dried in ambient condition. After that, silver nanoparticles were sintered in various conditions before measuring resistivity.

3.5.4 FT-IR microscope

Attenuated total reflection Fourier Transform Infrared (ATR FT-IR) spectroscopy technique was performed on Nicolet 6700 FT-IR spectrometer. Germanium was used as internal reflection element (IRE). The detector is mercury-cadmium-telluride (MCT) detector. Samples were prepared by placing a drop of samples solution on glass slide. After the sample solution was dried, spectrums were collected.

3.5.5 UV-Visible spectroscope

The quartz cuvette was washed by distilled water before collecting the spectrum. A reference of pure distilled water was collected as the blank sample. The light source of this instrument is Deuterium lamp (Bandwidth 200-850 nm). The USB2000 spectrophotometer was used as detector. The instrument setup is shown in Figure 3.3.



Figure 3.3 Ocean Optics Portable UV-Visible spectrometer

CHAPTER IV

RESULTS AND DISCUSSION

4.1 Silver nanoparticles synthesis method as conductive ink.

Silver nanoparticles were synthesized by the chemical reduction of silver nitrate with sodium borohydride (NaBH_4). The molar ratio of $[\text{NaBH}_4]/[\text{AgNO}_3]$ (denoted as R) was varied in order to investigate the appropriate condition for silver nanoparticles synthesis.

Table 4.1 Condition in silver nanoparticles synthesized by chemical reduction method

$[\text{AgNO}_3]$ (mol/L)	$[\text{NaBH}_4]$ (mol/L)	R
0.186	0.130	0.7
0.186	0.167	0.9
0.186	0.186	1.0

The complete of reaction was examined by adding NaBH_4 into the supernatant. For $R = 0.7$, the color of supernatant was changed from colorless to yellow and UV-Visible spectrum showed maximum intensity at 400 nm. In case of $R = 0.9$, UV-Visible spectrum showed the increase of absorption peak at 360 nm. These results indicated that there was a lot of silver ion in the supernatant. Both reactions were incomplete due to the inadequate concentration of reducing agent.

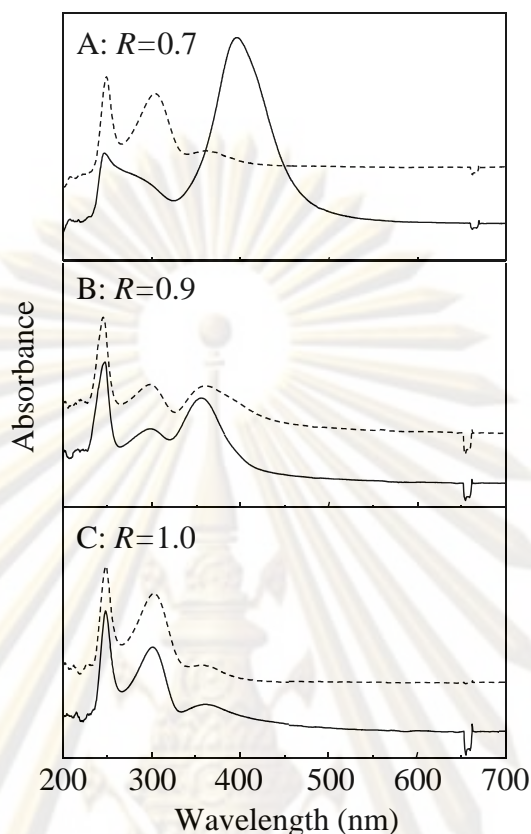


Figure 4.1 UV-Visible spectrum of supernatant at (A) $R = 0.7$, (B) $R = 0.9$, and (C) $R = 1.0$. The (---) represent supernatant before adding NaBH_4 , and (—) represent supernatant after adding NaBH_4 .

The optimum ratio for synthesizing silver nanoparticles was 1.0. When NaBH_4 was added into supernatant, changing of absorption peak around 360 nm did not occur.

In case of conductive silver ink, the silver nanoparticles must have no residual ion such as nitrate (NO_3^-), borate (BO_3^{3-}), and sodium ion (Na^+) have to be excluded from the colloidal silver nanoparticles. When silver was dried on substrate, these ions can form salt crystals, which preferably absorb the moisture. The moisture led to short circuit when the electrical circuit was closed.

Since, nitrate ions are soluble in water. After separating silver nanoparticles from supernatant, most of the nitrate ions still dissolve in supernatant. The result of FT-IR spectrum showed sharp peak around 820 cm^{-1} as shown in Figure 4.2A and 4.2B indicated that more inorganic nitrate salt existed in supernatant and washing solution. But the spectrum from Figure 4.2C did not show any peak around this region. These results implied that nitrate could be completely eliminated from silver nanoparticles after washing with distilled water.

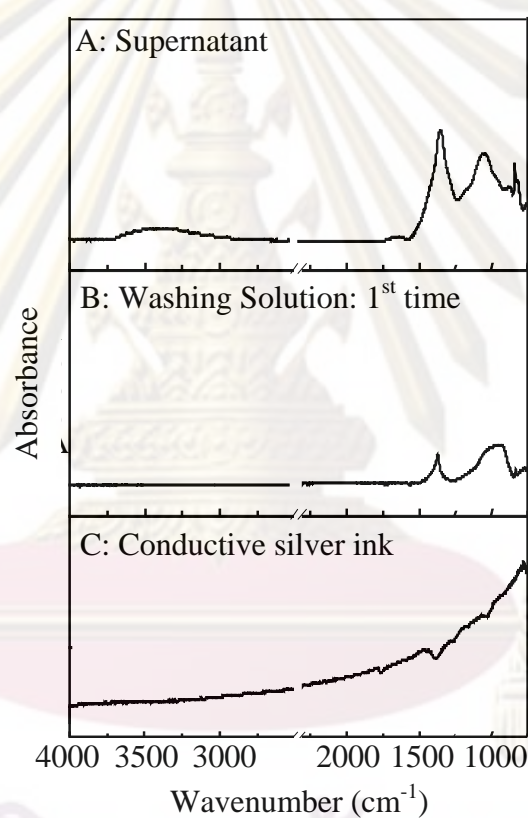


Figure 4.2 FT-IR spectrum of (A) supernatant, (B) washing solution and (C) conductive silver ink.

FT-IR spectrum from Figure 4.2A and 4.2B showed a peak at 1340 cm^{-1} which indicated B-O stretching vibration. These results indicated that most borate ions dissolved in the supernatant and washing solution. However, borate ions were also eliminated from silver nanoparticles by separation of supernatant and washing silver nanoparticles with distilled water. Therefore, silver nanoparticles were purified by centrifugation and repeatedly washed silver nanoparticles with distilled water. Most of the useless residual in silver nanoparticles could be extracted by water.

After purification, silver nanoparticles were redispersed into a suitable dispersing agent i.e. 0.1 % (w/v) trisodium citrate solutions with ultrasonic mixture to adjusted the final concentration of silver particles. The optimum concentration of silver nanoparticles for applying as conductive silver ink was more than 100,000 ppm or 10 wt. %. TEM images from Figure 4.3 showed spherical silver nanoparticles with diameter approximately 5 nm.

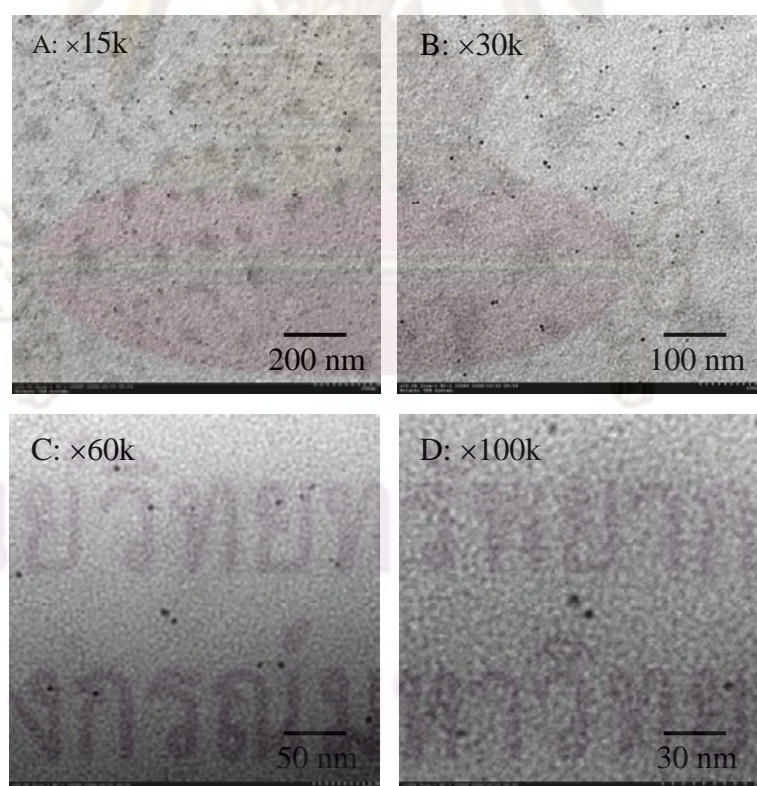


Figure 4.3 TEM images of conductive silver ink.

The conductive ink made of silver nanoparticles was developed for stamp printing, screen printing, and demonstration of conductive pen. When conductive silver ink was dried on substrate and connected to power supply, the ink became conductive and could light the LED as shown in Figure 4.4C.

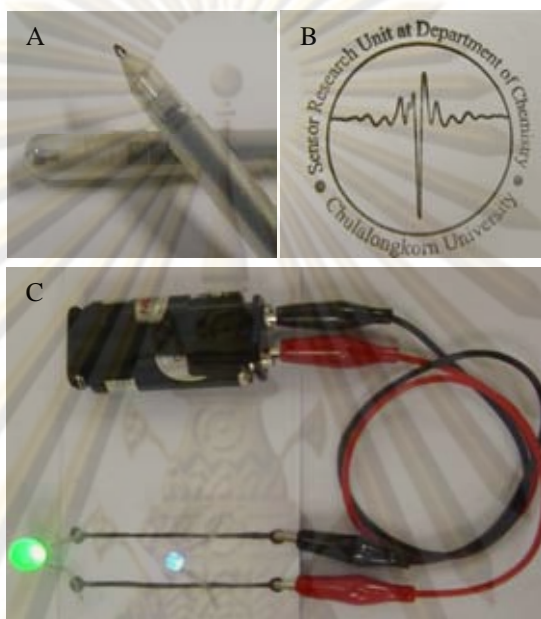


Figure 4.4 (A) Conductive pen, (B) stamp printing, and (C) LEDs lid after silver film were connected with the power supply.

Summary

The appropriate method for synthesized conductive silver ink could be summarized into three steps. The first step was synthesized silver citrate complex by reaction of silver salt with trisodium citrate. The second step was synthesized silver nanoparticles by redox reaction in three-ways connection tube reactor and the optimum molar ratio of sodium borohydride to silver nitrate was 1.0. Finally were purification and redispersed into the suitable solution. Silver nanoparticles were separated from supernatant by centrifugation and repeatedly washed with distilled water. Silver nanoparticles were redispersed into 0.1 % (w/v) trisodium citrate solution for used as conductive ink. When conductive silver ink was dried on substrate, silver film was showed conductive property.

4.2 The effect of stabilizer concentration on the size of silver nanoparticles.

When silver citrate complex particles were synthesized by silver nitrate with trisodium citrate without soluble starch as the stabilizer, aggregation and precipitation of silver citrate complex could be observed. In this work, soluble starch was used as stabilized silver citrate complex particles. Concentration of soluble starch was varied from 0.10, 0.25 and 0.50 % (w/v) as shown in Figure 4.5B, 4.5C, and 4.5D, respectively. The results in Figure 4.5 suggested that the increase in trisodium citrate concentration was the increase in precipitation of silver citrate complex. For, conductive silver ink, the lowest concentration of stabilizer was investigated.



Figure 4.5 Silver citrate complex at various concentration (A) without starch, (B) 0.10 % (w/v), (C) 0.25 % (w/v), and (D) 0.50 % (w/v) starch. The molar ratio of trisodium citrate dihydrate to silver nitrate, $[\text{trisodium citrate}]/[\text{AgNO}_3]$ was increased from 0, 4.0×10^{-3} , 8.0×10^{-3} , 1.6×10^{-2} , and 3.2×10^{-2} , respectively.

Therefore, 0.10 % (w/v) of soluble starch was used to stabilize silver citrate complex particles. The molar ratio of trisodium citrate dihydrate to silver nitrate was varied from 4.0×10^{-3} , 8.0×10^{-3} , 1.6×10^{-2} , and 3.2×10^{-2} . Size, size distribution and morphology were observed by AFM.



Figure 4.6 The photographic images of (A) Silver citrate complex that had [trisodium citrate]/[AgNO₃] from 4.0×10^{-3} , 8.0×10^{-3} , 1.6×10^{-2} , and 3.2×10^{-2} , respectively and (B) silver nanoparticles were synthesized from silver citrate complex with NaBH₄.

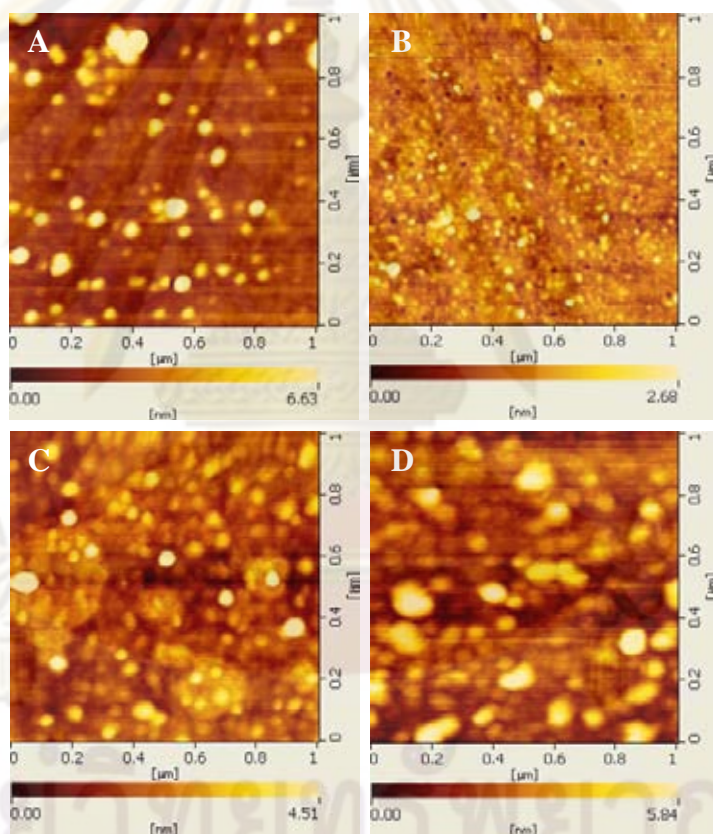


Figure 4.7 AFM images of silver particles at various [trisodium citrate]/[AgNO₃], (A) without citrate, (B) 4.0×10^{-3} , (C) 8.0×10^{-3} , and (D) 1.6×10^{-2} . Silver nanoparticles size were in the range of 30-60, 5-30 nm, 30-50 nm, and 30-80 nm, respectively.

When trisodium citrate was absent, the synthesized nanoparticles exhibited size in the range of 30-60 nm. Silver salt was reduced to Ag^0 and grew to the larger particles. However, silver nanoparticles were stabilized in starch solution. The proposed mechanism for formation silver nanoparticles is as follows:

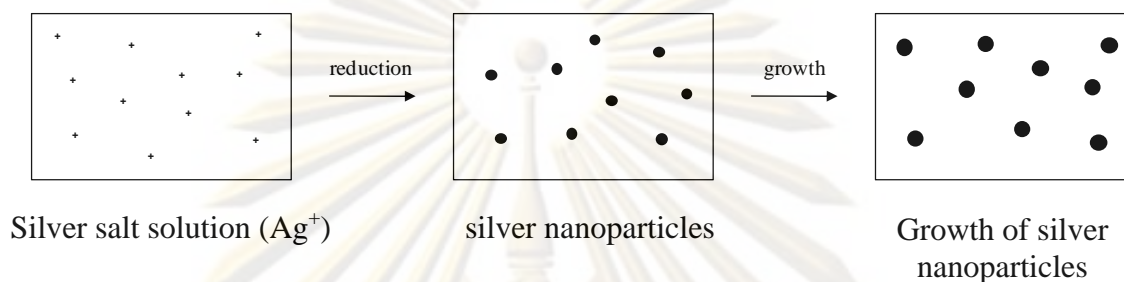
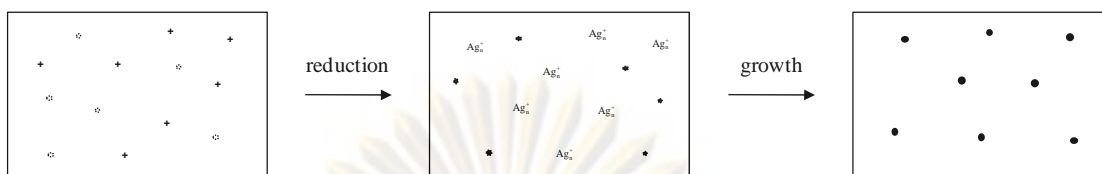


Figure 4.8 Schematic diagram of mechanism for formation of silver nanoparticles without trisodium citrate.

With trisodium citrate as stabilizer, different mechanism was proposed. When $[\text{trisodium citrate}]/[\text{AgNO}_3]$ was 4.0×10^{-3} , less silver citrate complex was incompletely formed. In addition, most composition in solution was silver salt (Ag^+). After the redox reaction, Ag^+ form silver citrate complex could be reduced to Ag^0 on citrate. Free silver ion was reduced to Ag^0 and then underwent condensation to form oligomeric cluster (Ag_n^+). In the reaction proceeds, oligomeric cluster was preferentially grown on Ag^0 that binding with citrate [47]. The synthesized silver nanoparticles possessed the size range of 5-30 nm as revealed by AFM images as shown in Figure 4.7B.

A: $[\text{trisodium citrate}]/[\text{AgNO}_3] = 4.0 \times 10^{-3}$

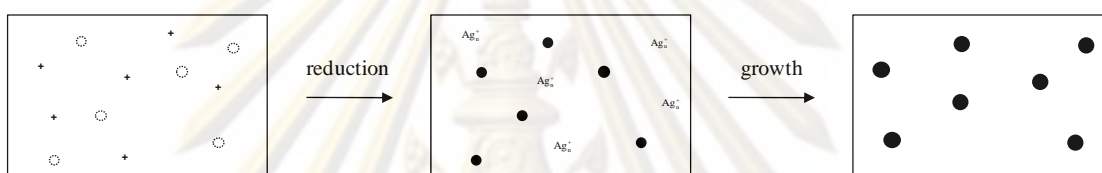


Silver citrate complex and Ag^+ dissolved in 0.1% (w/v) soluble starch

Formation of oligomeric cluster and Ag^0 on citrate compound

Oligomeric cluster adsorbed and growth on Ag^0 that adsorb on citrate compound

B: $[\text{trisodium citrate}]/[\text{AgNO}_3] = 8.0 \times 10^{-3}$



Large size of silver citrate complex and Ag^+ dissolved in 0.1% (w/v) soluble starch

Formation of oligomeric cluster and Ag^0 on citrate compound

Oligomeric cluster adsorbed and growth on Ag^0 that adsorb on citrate compound

Figure 4.9 Schematic diagram of formation of silver nanoparticles mechanism with $[\text{trisodium citrate}]/[\text{AgNO}_3]$ equal to (A) 4.0×10^{-3} and (B) 8.0×10^{-3} before redox reaction occurred.

When $[\text{trisodium citrate}]/[\text{AgNO}_3]$ was 8.0×10^{-3} , the larger particles of silver citrate complex were formed [31, 46] because 0.10 % (w/v) of soluble starch could not protect aggregation of silver citrate complex particles. Most free silver ion still existed in the solution. After redox reaction had occurred, silver ion in silver citrate complex was reduced to Ag^0 on citrate. The free silver ion was reduced to Ag^0 and condensed to oligomeric cluster and then prefer growth on Ag^0 binding with citrate. As a result, the aggregation of silver citrate complex leading to the larger silver nanoparticles which were in the size range of 30-50 (Figure 4.7C). The increase in $[\text{trisodium citrate}]/[\text{AgNO}_3]$ would increase in size of silver nanoparticles. When $[\text{trisodium citrate}]/[\text{AgNO}_3]$ was equal to 1.6×10^{-2} , size of silver nanoparticles was in the range of 30-80 nm as observed by AFM (Figure 4.7D).

When, [trisodium citrate]/[AgNO₃] was more than 3.2×10^{-3} , soluble starch concentration of 0.10 % (w/v) could not stabilize silver citrate complex. As a result, precipitation of silver citrate complex occurred. Therefore, this condition did not appropriate for silver nanoparticles synthesis.

Summary

The smallest size of silver nanoparticles was synthesized by reduction of silver citrate complex at [trisodium citrate]/[AgNO₃] was equal to 4.0×10^{-3} with NaBH₄. The results from AFM images indicted that the size of silver particles is about 5-30 nm. The increase in concentration of trisodium citrate is the increase in size of silver particles.



ศูนย์วิทยทรัพยากร
จุฬาลงกรณ์มหาวิทยาลัย

4.3 Sintering of phenomenon of conductive ink made of silver nanoparticles.

Generally, sintering phenomenon is temperature dependence. In 2006, Dongjo Kim et al [1]. could develop a conductive silver ink applicable to ink-jet printing. Silver nanoparticles were synthesized by chemical reduction method. The size of silver nanoparticles was 20 nm. The silver loading in conductive ink was in the range of 20 wt. %. After heat-treatment at 100-300 °C for 30 min, the size of silver particles was in the range of 200-500 nm. In 2006, microwave sintering of conductive silver tracks was studied by Jolke Perelaer et al [3]. Silver nanoparticles were dispersed in tetradecane. The nanopaste contains 57.8 wt. % of silver nanoparticles which the particle diameters was in the range of 5-10 nm. After the silver film was heated with microwave, the size of silver particles was in the range of 50-200 nm. The results from Dongjo Kim et al. and Jolke Perelaer et al. indicated that silver nanoparticles were sintered to the larger particles by thermal-treatment.

The sintering phenomenon could also occur at room temperature. In this work, sintering phenomenon was studied by changing the concentration of conductive silver ink. According to sintering mechanism, each particle moved toward to the center of another particle and then two particles were merged together. As a result, the neckings between the particles were formed. When sintering was completed, the larger particles were observed.

After synthesis and purification, silver nanoparticles were redispersed into 0.10 % (w/v) trisodium citrate solution and concentration of silver nanoparticles was adjusted to 100,000 ppm or 10 wt. %. It is assumed that silver nanoparticles can separate from solution completely. To study room temperature sintering phenomenon, conductive silver ink was diluted to 1 ppm, 10 ppm, 100 ppm, 1,000 ppm, 10,000 ppm and 100,000 ppm concentration. The results from AFM images as shown in Figure 4.10A and 4.10B indicated that at low concentration of conductive silver ink; 1 ppm and 10 ppm, the average size of silver particles was 10 nm. At 100 ppm,

the AFM images of silver film showed various particles sizes i.e. 10 nm, 20 nm, and 50 nm. The larger particles were formed by sintering of smaller particles.

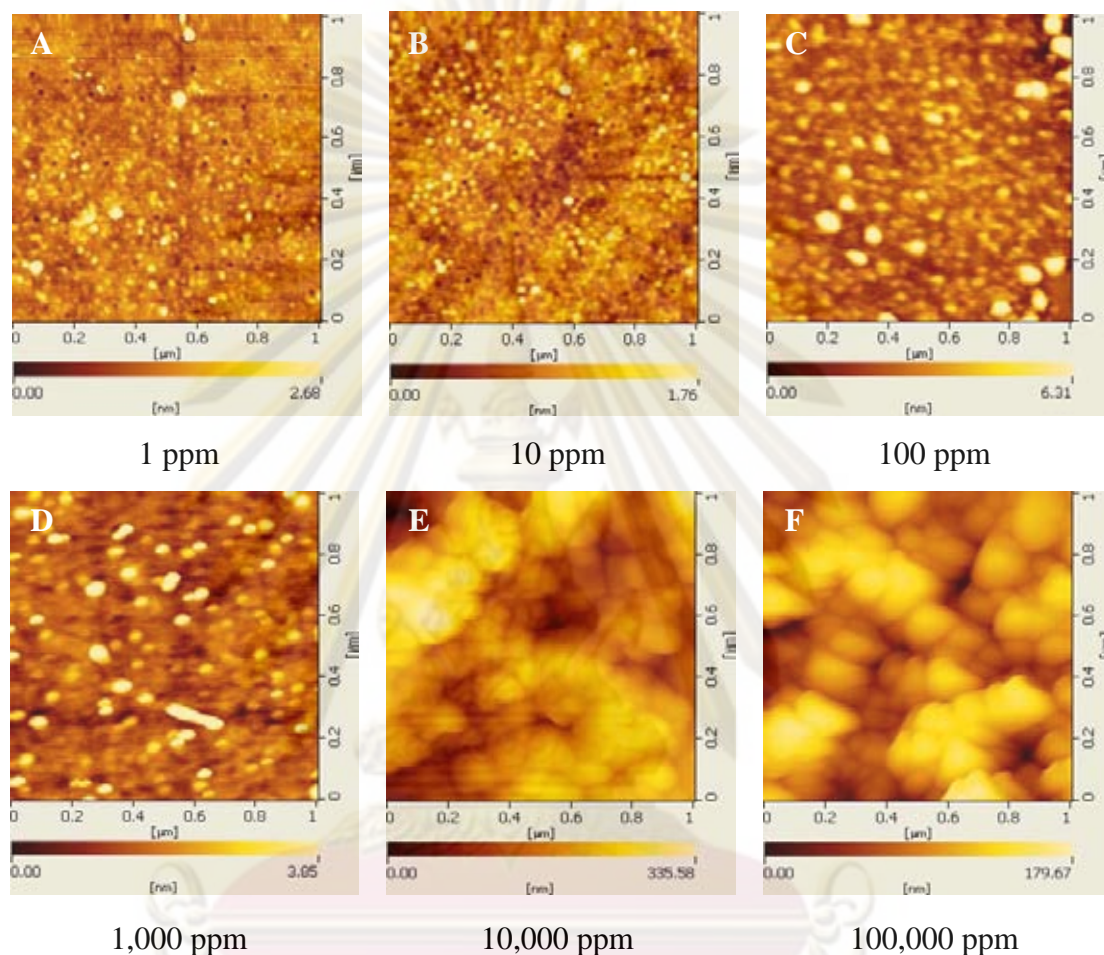


Figure 4.10 AFM images of silver film at (A) 1 ppm, (B) 10 ppm, (C) 100 ppm, (D) 1,000 ppm, (E) 10,000 ppm, and (F) 100,000 ppm.

Silver film of conductive silver ink at concentration of 1,000 ppm showed the average sizes of silver nanoparticles about 40 nm because of the sintering effect. However, silver film did not conduct because silver nanoparticles did not connect to the other silver particles. When silver 10,000 ppm was dried on substrate, original silver particles could sinter because the average size of particles grew up to 100 nm, but silver load was not enough to sinter all over film. Therefore, in this concentration, silver film could not show the conductive property.

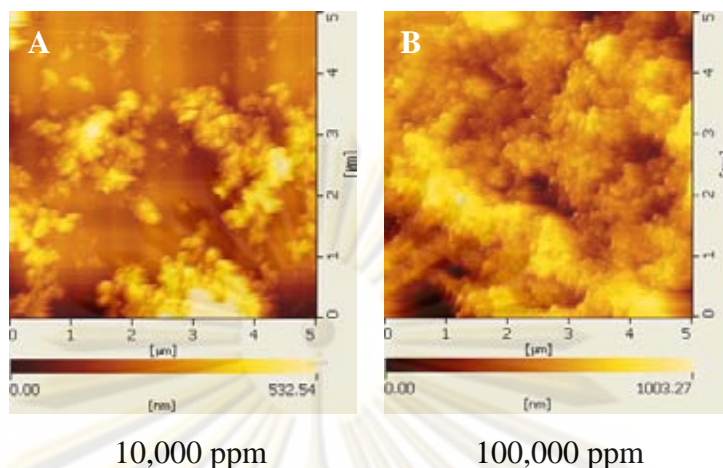
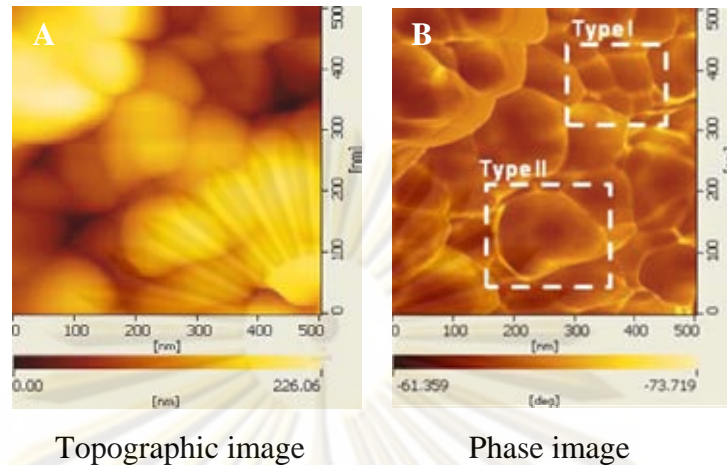


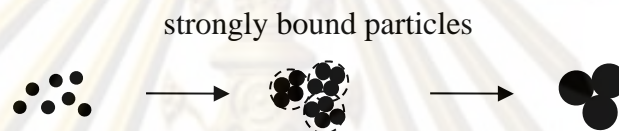
Figure 4.11 AFM images of silver nanoparticles at (A) 10,000 ppm and (B) 100,000 ppm.

The silver film showed conductivity when conductive silver ink was more than 100,000 ppm. After sintering, the average size of silver particle was 100 nm as shown in Figure 4.11B. When conductive silver ink deposited on substrate, the solvent was eliminated and electrical conductivity was enabled by high silver load and sintering phenomenon.

Silver particles after sintering have the irregular size and shape because the difference of sintering mechanism could be derived into two main types, surface change mechanism and rearrangement mechanism. In surface change mechanism, the particles were fused together by strongly bound and the particles were compacted together. In rearrangement mechanism, weakly bound between particles was formed and the primary particles could rearrange before agglomeration. However, in this study both sintering mechanisms occurred after silver nanoparticles were dried on substrate.



Type I: Surface area change mechanism



Type II: Rearrangement mechanism



Figure 4.12 (A) AFM image of silver nanoparticles at 100,000 ppm after sintering. (B) Phase image of Figure 4.12A. Type I and Type II represent the type of sintering mechanisms.

After silver particles sintered, differences of particles size were observed. When silver nanoparticles sintered by surface change mechanism, the obtained particles were smaller than those obtained by rearrangement mechanism. The surface change mechanism, silver particles could sinter with the nearest particles due to bonds between particles were strong and the limitation of particles size, silver particles could not sinter more than this. Therefore, the size of sintered silver particles depended on the amount of neighbor silver particles. In case of rearrangement mechanism, silver particles could rearrange due to bounds between particles were weak. As a result, the

larger size was observed. However, when temperature were increased by heat-treatment, silver particles could more sinter as shown in Figure 4.13B and 4.13C.

In order to study the effect of heat-treatment temperatures and heat-treatment times on silver film of conductive silver ink, sintering conditions were varied from room temperature to 100 °C for 10 min. and 200 °C for 120 min. In addition, the effect of mechanical rubbing was investigated. The morphology changes were observed by AFM.

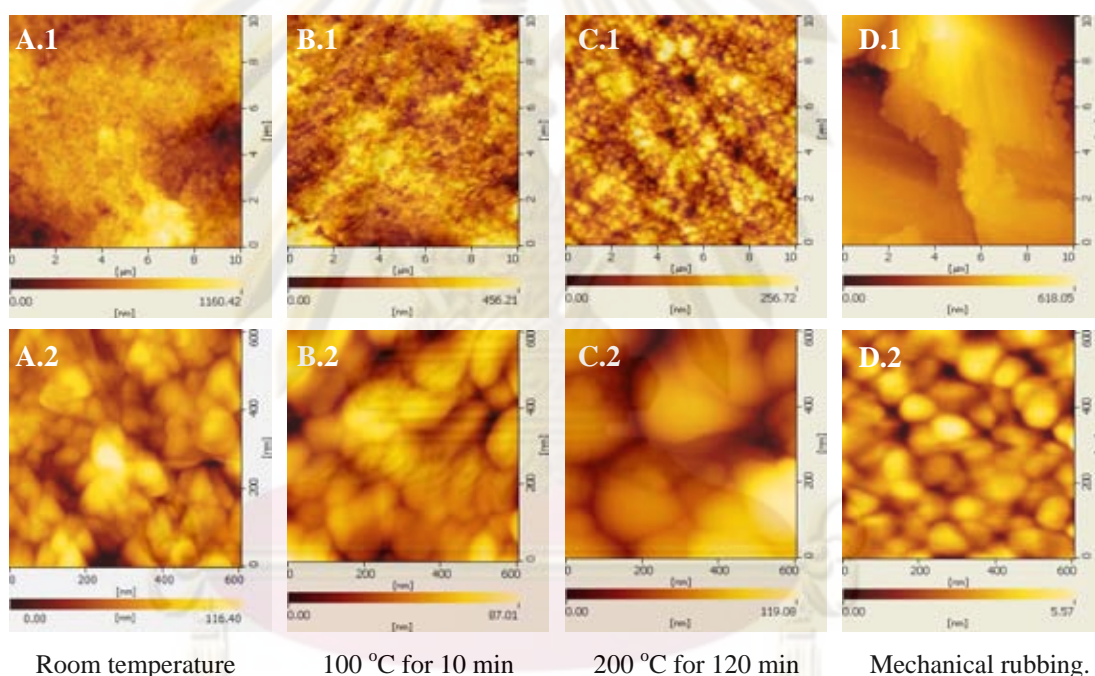


Figure 4.13 AFM images of silver nanoparticles after sintering at various conditions; (A) room temperature, (B) 100 °C, for 10 min., (C) 200 °C, for 120 min., and (D) mechanical rubbing.

Table 4.2 Sheet resistivity of silver particles after sintering at various conditions.

Sintering condition	Sheet resistivity (Ω/mil^2)
Room temperature	0.613
100 °C, for 10 min.	0.021
200 °C, for 120 min.	0.005
Mechanical rubbing	0.016

AFM images in Figure 4.13 show topography of silver nanoparticles after sintering at various conditions. At room temperature sinter, the average particles size was increased from 10 nm to 50 nm and sheet resistivity of silver film was 0.613 Ω/mil^2 . After heat treatment at 100 °C for 10 min., average size of silver nanoparticles was 100 nm. However, small numbers of smaller particles (50 nm) were also existed. In this condition, sheet resistivity was 0.021 Ω/mil^2 . When heat-treatment temperature and heat-treatment time were increased to 200 °C for 120 min., average size of silver particles after sintering was 200 nm. Decreasing of sheet resistivity to 0.005 Ω/mil^2 was observed.

At room temperature silver nanoparticles could sinter to larger particles. Size of silver particle increased with the increasing heat-treatment temperature and heat-treatment time. Resistivity could be decreased with the increasing sintering temperature and sintering time because particles contact area was increased by sintering phenomena. The increased conductivity in silver film has two import factors, increase in contact between particles and increasing particles contact area. The increased contact between particles was made by increased the silver loading. The increased particles contact area was made by sintering.

In case of mechanical rubbing, AFM image clearly showed closely packed of silver film. But the size of silver particles did not change after rubbing. This result

indicated that contacts between particles were increased or coordination number of silver particles was increased. The sheet resistivity of silver film after mechanical rubbing was $0.016 \Omega/\text{mil}^2$ which less than sheet resistivity of silver film at room temperature. The increase of contact between particles led to resistivity drop. The size of silver nanoparticles did not change due to the sintering phenomenon was not occurred by mechanical rubbing.

Summary

High silver loading and small size of silver particles enable the room temperature sintering at conductive silver ink. After dilution of conductive silver ink to 1 ppm, a size of silver particles was 5-30 nm. When conductive ink was dried on substrate the larger particles were observed. Silver film began sintering at 100 ppm concentration. At high concentration (100,000 ppm), silver loading was high enough to allow adjacent silver particles to gain contact upon drying. The silver film became conductive when the concentration of silver nanoparticles in the conductive ink was more than 100,000 ppm. The conductivity of silver film could be improved by thermal treatment or by mechanical rubbing.

CHAPTER V

CONCLUSIONS

Conductive silver ink was synthesized by chemical reduction of silver nitrate with sodium borohydride. Trisodium citrate was used as stabilizer. After synthesis, colloid silver nanoparticles were purified and redispersed into 0.1 % (w/v). The silver loading of conductive silver ink was 10 wt. %. From AFM images, it is concluded that the synthesized silver nanoparticles have spherical shape with an average diameter of 10 nm. The increase in concentration of stabilizer is the increase in size of silver particles. After silver nanoparticles sintering on the substrate, an average size of silver particles was 100 nm. The sheet resistivity of silver film was $0.613 \Omega/\text{mil}^2$. The silver film was made highly conductive by thermal treatment or by mechanical rubbing. The conductive silver ink could be made into the conductive circuit by stamp printing, screen printing, drop-on-demand printing and demonstration of conductive pen. It can be applied on the temperature-sensitive substrates such as thin film polymer and paper without deforming or destroying the substrate.

ศูนย์วิจัยทรัพยากร
จุฬาลงกรณ์มหาวิทยาลัย

REFERENCES

- [1] Kim D. et al. Organic thin film transistor using silver electrodes by the ink-jet printing technology Thin Solid Films 515 (2007): 7692-7696.
- [2] Park J.; Baek S. Thermal behavior of direct-printed lines of silver nanoparticles Scripta Materialia 55 (2006): 1139-1142.
- [3] Perelaer J.; Gans B.; Schubert U.S. Ink-jet printing and microwave sintering of conductive silver tracks Adv. Matter 18 (2006): 2101-2104.
- [4] Ryu B. et al. Synthesis of highly concentrated silver nanosol and its application to inkjet printing Colloid and Surface A 270 (2005): 345-351.
- [5] Magdassi S. et al. Silver nanoparticles as pigments for water-based ink-jet inks Chem. Matter. 15 (2003): 2208-2217.
- [6] Pudas M. et al. Gravure printing of conductive particulate polymer inks on flexible substrates Progress in Organic Coatings 54 (2005): 310-316.
- [7] Pudas M.; Hagberg J.; Leppavuori S. Printing parameters and ink components affecting ultra-fine-line gravure-offset printing for electronics applications J. Euro. Cera. Soc. 24 (2004): 2943-2950.
- [8] Yin S.; Farschi R.; Subramanian V. An ink-jet-deposited passive component process for RFID IEEE Transactions on electron device 51 (2004): 1978-1983.
- [9] Kolbe J. et al. Inkjettable conductive adhesive for use in microelectronics and Microsystems technology Microelectronics Reliability 47 (2007): 331-334.
- [10] Greer J. R.; Street R. A. Thermal cure effects on electrical performance of nanoparticles silver ink Acta Materialia 55 (2007): 6345-6349.
- [11] Wakuda D.; Kim K.; Sukanuma K. Room temperature sintering of Ag nanoparticles by drying solvent Scripta Materialia 59 (2008): 649-652.
- [12] Pradhan N.; Pal A.; Pal T. Silver nanoparticles catalyzed reduction of aromatic nitro compounds Colloid and Surface A 196 (2002): 247-257.

- [13] Munro C. H.; Smith W. E.; Garner M.; Clarkson J.; White P. C. Characterization of the Surface of a Citrate-Reduced Colloid Optimized for Use as a Substrate for Surface-Enhanced Resonance Raman Scattering Langmuir 11 (1995): 3712-3720.
- [14] Cao Y. C.; Jin R.; Thaxton C. S.; Mirkin C. A. A two-color-change, nanoparticle-based method for DNA detection Talanta 67 (2005): 449-455.
- [15] Zhao J.; Zhang X.; Yonzon C. R.; Haes A. J.; Van Duyne R. P. Localized surface plasmon resonance biosensors Nanomedicine 1 (2006): 219-228.
- [16] Pal S.; Tak Y. K.; Song J. M. Does the antibacterial activity of silver nanoparticles depend on the shape of the nanoparticle? A Study of the Gram-Negative Bacterium *Escherichia coli* Appl. Environ. Microbiol. 73 (2007): 1712-1720.
- [17] Panáček A. et al. Silver colloid nanoparticles: synthesis, characterization, and their antibacterial activity J. Phys. Chem. B 110 (2006): 16248-16253
- [18] Sondi I.; Salopek-Sondi B. Silver nanoparticles as antimicrobial agent: a case study on *E. coli* as a model for Gram-negative bacteria J. Colloid Interface Sci. 275 (2004): 177-182.
- [19] Willets K. A.; Van Duyne R. P. Localized surface plasmon resonance spectroscopy and sensing Annu. Rev. Phys. Chem. 58 (2007): 67-97.
- [20] Kelly K. L.; Coronado E.; Zhao L. L.; Schatz G. C. The optical properties of metal nanoparticles: the influence of size, shape, and dielectric environment J. Phys. Chem. B 107 (2003): 668-677.
- [21] Wiley B. J. et al. Maneuvering the surface plasmon resonance of silver nanostructures through shape-controlled synthesis J. Phys. Chem. B 110 (2006): 15666-15675.
- [22] Kreibig U.; Vollmer M. Optical properties of metal clusters Springer Berlin, Germany, 1995.
- [23] Haes A. J. et al. A nanoscale optical Biosensor: the long range distance dependence of the localized surface Plasmon resonance of noble metal nanoparticles J. Phys. Chem. B 108 (2004): 109-116.

- [24] Draine T. B.; Flatau P. J.; Discrete-dipole approximation for scattering calculations J. Opt. Soc. Am. A 11 (1994): 1491-1499.
- [25] Takagi M. Electron-diffraction study of liquid-solid transition of thin metal films J. Phys. Soc. Jpn. 9 (1954): 359-363.
- [26] Martin C. J. et al. An experimental test of Lindemann's melting law J. phys. C 10 (1977): 3521-3526.
- [27] Shi F. G. Pendant thermal vibrations and melting in nanocrystals J. Mater. Res. 9 (1994): 1307-1313.
- [28] Weber A. P.; Friedlander S.K. In situ determination of the activation energy for restructuring of nanometer aerosol agglomerates J. Aerosol Sci. 28 (1997): 179-192.
- [29] Nakaso K. et al. Evaluation of the change in the morphology of gold nanoparticles during sintering Aerosol Science 33 (2002): 1061-1074.
- [30] Frenkel J. Viscous flow of crystalline bodies under the action of surface tension J Phys. 9 (1945): 385-391.
- [31] Pillai Z. S.; Kamat P.V. What factors control the size and shape of silver nanoparticles in the citrate ion reduction method? J. Phys. Chem. B 108 (2004): 945-951.
- [32] Silvert P. Y.; Herrera-Urbina R.; Tekaiia-Elhsissena K. Preparation of colloidal silver dispersions by the polyol process Part 2. Mechanism of particle formation J. Mater. Chem. 7 (1997): 293-299.
- [33] Panacek A. et al. Silver colloid nanoparticles: synthesis, characterization, and their antibacterial activity J. Phys. Chem. B 110 (2006): 16248-16253.
- [34] Panigrahi S.; Kundu S.; Ghosh S. K.; Nath S.; Pal T. General method of synthesis for metal nanoparticles J. Nanoparticle Res. 6 (2004): 411-414.
- [35] Huang Z. Y.; Mills G.; Hajek B. Spontaneous formation of silver particles in basic 2-propanol J. Phys. Chem. 97 (1993): 11542-11550.
- [36] Pal T.; Sau T. K.; Jana N. R. Reversible formation and dissolution of silver nanoparticles in aqueous surfactant media Langmuir 13 (1997): 1481-1485.

- [37] Shirtcliffe N.; Nickel U.; Schneider S. Reproducible preparation of silver sols with small particle size using borohydride reduction: for use as nuclei for preparation of larger particles J. Colloid Interface Sci. 211 (1999): 122-129.
- [38] Zukoski C. F. Formation mechanisms and aggregation behavior of borohydride reduced silver particles Langmuir 14 (1998): 7034-7046.
- [39] Huang H. H. et al. Photochemical formation of silver nanoparticles in Poly(N-vinylpyrrolidone) Langmuir 12 (1996): 909-912.
- [40] Gutierrez M.; Henglein A. formation of colloidal silver by "Push-Pull" reduction of Ag^+ J. Phys. Chem. 97 (1993): 11368-11370.
- [41] Turker M. Effect of production parameters on the structure and morphology of Ag nanopowders produced by inert gas condensation Mater. Sci. Eng. A 367 (2004): 74-81.
- [42] Mafune F.; Kohno J.; Takeda, Y.; Kondow T. Structure and stability of silver nanoparticles in aqueous solution produced by laser ablation J. Phys. Chem. B 104 (2000): 8333-8337.
- [43] Plum T. C. et al. Solid silver particle production by spray pyrolysis J. Aerosol Sci. 24 (1993): 383-392.
- [44] Carpick R.; Salmeron M. Scratching the surface: fundamental investigation of tribology with atomic force microscopy Chem. Rev. 97 (1997): 1163-1194.
- [45] Davis L. M.; Thompson D.W. Novel and Facile Approach to the Fabrication of Metal-Patterned Dielectric substrate Chem. Mater. 19 (2007): 2299-2303.
- [46] Djokić S. Synthesis and antimicrobial activity of silver citrate complexes Bioinorg. Chem. Appl. (2008): 1-7.
- [47] Mpourmpakis G.; Vlachos D. G. Insights into the Early Stages of Metal Nanoparticles Formation via First-Principle Calculation: the Roles of Citrate and Water Langmuir 24 (2008): 7465-7473.

CURRICULUM VITAE

Name: Mr. Chutiparn Lertvachirapaiboon

Date of Birth: December 28, 1984 **Birth place:** Bangkok, Thailand

Address: 3/1102, Phaholyothin road, Bangkhen, Bangkok 10220, Thailand,
E-mail address: l_chutiparn@hotmail.com

Education:

2007 Bachelor of Science in Chemistry
King Mongkut's University of Technology Thonburi, Thailand

2009 Master of Science in Chemistry
Chulalongkorn University, Thailand

Conferences:

January 30-February 1, 2008	Pure and Applied Chemistry International Conference 2008, Thailand
March 13-14, 2008	The Science Forum 2008, Thailand
April 22-25, 2008	International Conference on Smart Materials Smart/Intelligent Materials and Nanotechnology and 2 nd International Workshop on Functional Materials and Nanomaterials, Thailand
June 18-19, 2008	Yonsei University-Chulalongkorn University The 2 nd Joint Symposium, Korea
October 16-17, 2008	The 2 nd Thailand Metallurgy Conference, Thailand
October 31-November 1, 2008	34 th Congress on Science and Technology of Thailand (STT34), Thailand
December 17-19, 2008	4 th Mathematic and Physical Science Graduate Congress, Singapore

Conferences:

January 14-16, 2009	Pure and Applied Chemistry International Conference 2009, Thailand
September 1-3, 2009	ChinaNANO2009, China

Awards:

January 30-February 1, 2008	The most popular poster award in Pure and Applied Chemistry International Conference 2008, Thailand
March 13-14, 2008	Best presentation award in The Science Forum 2008, Thailand
2009	NRCT Admiral Award for Innovation, Entitled “Silver Nanoparticles Technology for Industrial Application”
2009	NRCT Grant for Model 2V-Research Program, Entitled “ Development of Commercial Prototype of Conductive Ink Made of Silver Nanoparticles”

ศูนย์วิจัยทรัพยากร
จุฬาลงกรณ์มหาวิทยาลัย